Bitlis Eren University Journal of Science and Technology

Contact:

Bitlis Eren University Journal of Science and Technology

Bitlis Eren University Journal of Science and Technology

Year: 2024 • Volume: 14 • Issue: 1

Editorial Board

Articles

SYNTHESIS AND CHARACTERIZATION OF CHROMIUM-BASED CATALYSTS ON TITANIUM-MODIFIED-MCM-41 FOR OXIDATIVE DEHYDROGENATION OF ISOBUTANE

Hiba Mustafa Yousef Mosa [1] (iD), **Meltem Dogan** [2] (iD), **Saliha Cetinyokus** [3, *] (iD)

[1] *Gazi University, Department of Chemical Engineering, Turkey,* hibamustafayousef.mosa@gazi.edu.tr
[2] *Gazi University, Department of Chemical Engineering, Turkey,* meltem@gazi.edu.tr
[3] *Gazi University, Department of Chemical Engineering, Turkey,* salihakilicarslan@gazi.edu.tr
*** *Corresponding author*

ABSTRACT

This study aimed to prepare chromium-based catalysts on titanium-modified MCM-41 for oxidative dehydrogenation reactions. MCM-41 was synthesized hydrothermally. In order to increase the hydrothermal stability of support, titanium was added to the MCM-41. The titanium source (K_2TiF_6) was dissolved in two different solvents (hot water and sulfuric acid). The hydrothermal stability test was performed with the samples. The samples were characterized by XRD, N_2 adsorption/desorption, FT-IR, and SEM/EDS analysis. When titanium was added to the MCM-41 structure, it was determined that the pore walls thickened, and the main peak characterizing the hexagonal structure was preserved. With the modification, the average pore diameter of MCM-41 decreased from 28Å to 22Å, and the surface area decreased from 1250 m^2/g to 500 m^2/g. The hydrothermal stability test indicated that the loading of titanium improved the stability of MCM-41. FT-IR results showed that titanium has formed strong bonds with oxygen atoms, creating Si-O-Ti, Ti-OH, and Ti-O bonds. These bonds enhanced to stabilize the MCM-41 structure, making it more resistant to structural changes. Smaller crystal size (178Å) and higher surface area (554 m^2/g) were determined in the support prepared by dissolving the titanium source in hot water. Therefore, this support was used in catalyst synthesis. Chromium-based catalysts on titanium-modified MCM-41 were prepared by wet impregnation method at different chromium loading (3% and 10%, by mass). The presence of the anatase phase of TiO_2 and inactive α-Cr_2O_3 in the high chromium-loaded sample was determined. Therefore, catalytic tests were carried out with a catalyst containing 3% chromium by mass, prepared using a Ti-modified support, as well as a catalyst prepared using an unmodified support. The highest isobutane conversion (94%) and isobutene selectivity (81%) values were obtained for catalyst supported on Ti-modified MCM-41. High activity predicted for catalyst supported on modified MCM-41 was explained by improving hydrophilic properties.

1   INTRODUCTION

Around 30 years ago, mesoporous MCM-41 materials were discovered and have been widely used in many applications, such as catalysis, adsorption, and separation technology [1]- [3]. MCM-41 has been extensively reported due to the high surface area (up to 1000 m2/g) and tailored mesoporous sizes (~10 nm) [4]. MCM-41 preparation method requires four ingredients: a silicate source, a surfactant molecule, acid, and water. The silica species that arise from the hydrolysis of the silicate source are negatively charged and are then attracted to the positively charged ammonium groups of the cationic surfactant [5], [6]. Cetyl Trimethyl Ammonium Bromide (CTAB) is the most often used surfactant in the synthesis. The surfactant is removed to reveal the mesoporous channels. There are different methods for removing the organic surfactant, such as solvent extraction or removal of physically adsorbed surfactants [7], electrochemical procedure [8], and UV/ozone irradiation [9]. However, the most widely used technique is burning organic templates in an air or oxygen atmosphere. This process generates surface silanol groups ($\equiv$Si-OH), as well as the formation of some fused siloxane bridges. However, the removal of the surfactant, coupled with the presence of an amorphous silica structure, leads to low structural stability for these mesoporous silicas [10]. The limited hydrothermal stability of MCM-41 refers to its susceptibility to damage from thermal treatments involving water, steam, or a combination of both. Bezerra et al. reported a systematic study on MCM-41 synthesized at various temperatures to relevant structural order of mesoporous silica under humidity. It was found that the stability of MCM-41 relied on pore wall thickness and the quantity of Si-OH groups when MCM-41 was exposed to humidity, water physisorption occurred, leading to a loss of structural order due to hydrolysis of siloxane bond [11]. A recent study by Perez et al. suggested that capillarity led to loss of ordering and structural damage of MCM-41 at moderate hydrothermal treatment temperatures in water, associated with hydrolysis and decreased mechanical strength [12].

Various methods have been developed to enhance the hydrothermal stability of MCM-41 materials, such as adding surfactant templates, using stable silica sources/precursors, grafting aluminum onto pure silica, creating thicker pore walls, eliminating silanol groups, and promoting silanol group condensation through salt or

hydrothermal structure-directing agents [12], [13]. Incorporating metal cations, such as Ti, Al, Cr, Zr, V, Mo, Cu, Ni, Co, and Fe, into the MCM-41 silica framework via controlled synthesis or post-synthesis modification enhances its catalytic properties and helps in overcoming the disadvantages mentioned above [3], [14]-[16]. Recently, the use of MCM-41 modified with Ti and Ti oxides has gained great attention in the industry. Due to its catalytic properties, it is widely used in basic catalytic processes such as environmental catalysis, petrochemical and refinery catalysis, olefin epoxidation, and biomass conversion [3], [17], [18]. Sekkiou et al. showed that Cu-MCM-41 exhibited low hydrothermal stability due to the addition of copper and the formation of CuO oxide; in contrast, Cu-Al-MCM-41 demonstrated high hydrothermal stability attributed to the presence of aluminum and an ion exchange process [19]. Chao et al. found that intercalation of the CuAAPTS complex improved hydrothermal stability by creating highly cross-linked silica "pillars" through covalent bonding [20]. Song et al. reported that pre-treatment with (NH4)2SiF6 improved hydrothermal stability by repairing surface defects and replacing some silicon hydroxyls with F-ions [21]. Jiang et al. showed that MCM-41 with Si/Al: 25 maintained its mesoporous structure even after a 12-hour hydrothermal stability test in boiling water due to the loading of the Al atom. This demonstrated that the hydrothermal stability of MCM-41 can be enhanced by secondary restructure with a pore diameter larger than 3.3 nm and a BET surface area exceeding 800 m^2/g [22].

Chromium-based catalysts are widely used in dehydrogenation reactions. Catalytic activity is high when the (+6) valence oxides of chromium are present in the catalyst structure. It was shown that the crystal size highly influenced the catalytic activity [23], [24]. Cr-based catalysts supported on Ti-doped MCM-41 materials exhibit improved structural properties. A study by Al-Awadi et al. stated that TiO2 modification of MCM-41 increased the stability [25]. Wan et al. confirmed that titanium loading in a Cr-based catalyst reduced hydrophobicity due to Si-Ti bond formation [26]. It was reported that titanium coating on the catalyst surface as a metal oxide produced a protective effect, preventing the leaching of the active species during the reaction [27].

The aim of this study was to synthesize chromium-based catalysts supported on titanium-modified MCM-41 for oxidative dehydrogenation of isobutane. It was predicted that the titanium modification positively improved hydrothermal stability

and active species distribution. Catalysts were prepared by wet impregnation method at different chromium loading (3% and 10%, by mass). It was decided to carry out the catalytic test with the catalyst containing 3% chromium by mass because of the low crystal size and high surface area. A catalyst was also prepared using an unmodified support to observe the effect of modification with titanium on catalytic activity.

2 EXPERIMENTAL

2.1 Synthesis of MCM-41 and Titanium-Modified-MCM-41

MCM-41 mesoporous silica was synthesized using $C_{19}H_{42}BrN$ (N-cetyl-N, N, N-trimethyl ammonium bromide) as surfactant and sodium silicate solution (composed of 27% SiO_2, 8% Na_2O, and 65% H_2O by mass) as the silica source. The synthesis was carried out with a surfactant/Si ratio of 0.5 (mole/mole). Firstly, the surfactant was dissolved in deionized water and stirred at 30°C until a clear solution was obtained. Then the sodium silicate solution was added dropwise under stirring. The resulting mixture's pH was adjusted to 11 before being placed in a Teflon-lined stainless-steel autoclave, where it was kept at 120°C for 96 hours. After removing the sample from the autoclave, it was washed, dried, and calcined in a dry air flow (135 ml/min) at 600°C for 6 hours.

To modify MCM-41, K_2TiF_6 (dipotassium hexafluorotitanate) was used as a titanium source. In the synthesis of titanium-modified MCM-41, the same method described above was followed in the synthesis of pure MCM-41. In the step where sodium silicate solution was added, the dissolved titanium source was added alternately with the silica source. The titanium source was dissolved in two different solvents (hot water and sulfuric acid). The synthesized samples were labeled as TiW-M (K2TiF6 dissolved in hot water) and TiA-M (K_2TiF_6 dissolved in acid).

The hydrothermal stability test was carried out for pure MCM-41 and samples of MCM-41 modified with titanium. First, the samples were put in 30 mL water and heated to 383K for 5 hours under gentle stirring. The amount of water was kept constant by adding hot water when needed. After this treatment, the remaining samples were filtered and dried at room temperature. Hydrothermally treated samples were named by writing "HT" at the end of their names.

2.2   Preparation of Chromium-Based Catalysts

In the catalyst preparation studies, chromium-based catalysts supported on titanium-modified MCM-41 were prepared by wet impregnation method with Cr(NO3)3.9H2O (chromium nitrate) as the chromium source. Chromium metal loading on the titanium-modified MCM-41 was planned to be 3% and 10% by mass, and titanium metal loading was kept constant at 2.5 % by mass. Deionized water was mixed with titanium-modified MCM-41, and then the dissolved chromium nitrate salt was added to the mixture drop by drop at 40°C. Then the mixture's temperature was raised to 60°C to evaporate the water followed by drying at 100°C. The prepared catalyst was calcined at 600°C for 6 hours with a dry air flow rate of 135 ml/min. The final obtained catalysts were denoted as xCr@Ti-MCM-41, where x represents the mass percentages of Cr. Using the impregnation method described above, the 3Cr@MCM-41 catalyst was also prepared using unmodified MCM-41.

2.3   Catalytic Tests

The activity of chromium-based catalysts used in the oxidative dehydrogenation of isobutane is highly affected by the crystal size, where the catalyst containing a smaller chromium crystal size shows better activity [28]. For this reason, it was decided to carry out the catalytic test studies with a 3Cr@Ti-MCM-41 catalyst, which had a smaller chromium crystal size. Catalytic test studies were also carried out with catalyst supported on unmodified MCM-41 (3Cr@MCM-41). The experimental setup used for the oxidative dehydrogenation of isobutane is given in Figure 1.
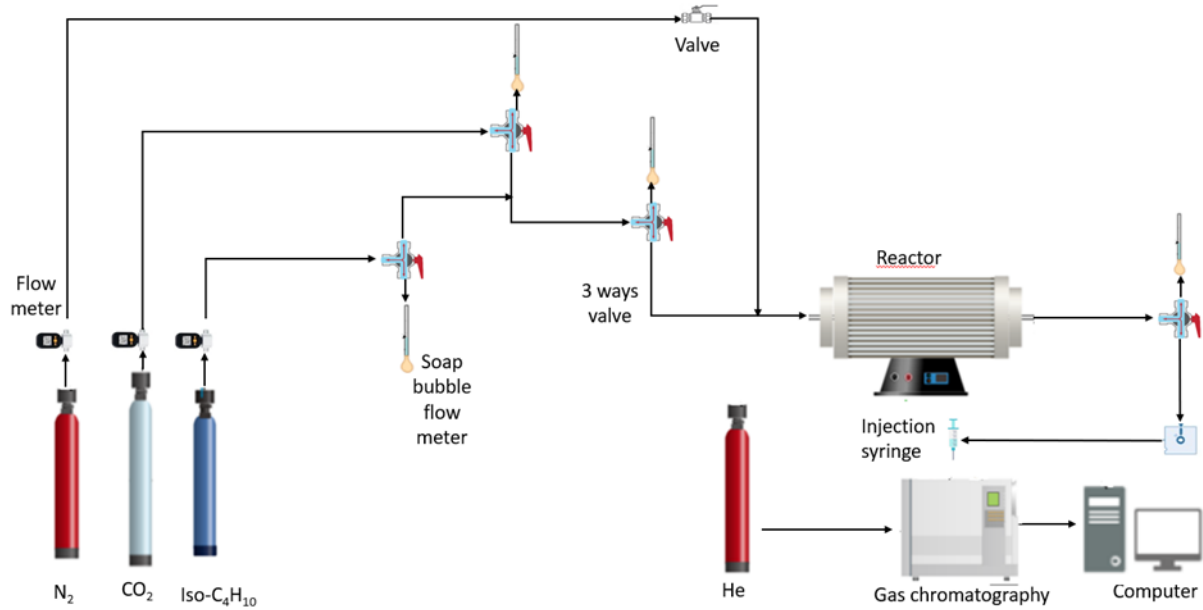
Figure 1. Experimental setup used for the catalytic tests

The catalytic tests were carried out in a quartz reactor (diameter: 0.65cm, length: 1cm) with a catalyst loading of 0.1 grams. The experiment was carried out at a temperature of 600°C and under atmospheric pressure for 2 hours. The feed, consisting of isobutane and carbon dioxide (i-C_4H_{10}/CO_2 feed ratio: 1/5), was fed to the reactor at a total flow rate of 50 ml/min (WHSV: 51 h⁻¹). The gas samples collected at specific time intervals from the reactor outlet were analyzed using a gas chromatography instrument (SRI 8610C) equipped with a silica column. The isobutane conversion and isobutene selectivity values were determined from the following equations (Eq.1 and Eq.2).

$$Isobutane\ conversion\ (\%) = \frac{\left(i\text{-}C_4H_{10,initial} - i\text{-}C_4H_{10,exit}\right)}{\left(i\text{-}C_4H_{10,initial}\right)} \times 100 \qquad \textbf{(1)}$$

$$Isobutene\ selectivity\ (\%) = \frac{\left(i\text{-}C_4H_{8,exit}\right)}{\left(i\text{-}C_4H_{10,initial} - i\text{-}C_4H_{10,exit}\right)} \times 100 \qquad \textbf{(2)}$$

2.4   Characterization Studies

2.4.1 XRD

XRD patterns of MCM-41 supports and catalysts were performed using a Rigaku instrument (D/MAX N2200) with Cu, Kα irradiation source (λ= 1.5406Å). Small angle profiles (2θ range: 1-10˚) were used to determine the characteristic peaks of MCM-41, while wide angle profiles (2θ range: 10-80˚) were used to identify distinct crystalline formations in metal-incorporated materials.

N_2 adsorption/desorption

The BET surface areas, pore size distribution, and pore volumes of the samples were determined through N_2 adsorption/desorption using the Quantochrome (Autosorp 6) physical adsorption device after degassing the samples at 250˚C for 2 hours. Pore size distributions were analyzed using the Barrett Joyner–Halenda (BJH) model from the branch of the adsorption profiles of isotherms.

2.4.2 SEM/EDS

SEM/EDS analyses were conducted using a QUANTA (400F Field Emission) high-resolution Scanning Electron Microscope (SEM). SEM photographs were used to analyze the samples' morphology, while EDS analyses determined the compositions of the samples.

2.4.3   FT-IR

Fourier Transform Infrared Spectrophotometer (Jasco FT-IR 4700) analyses were performed to identify the chemical bonds present in the Ti-modified MCM-41 structure.

3   RESULTS AND DISCUSSIONS

3.1   Characterization Studies of the Supports

Hydrothermal stability tests were performed to determine the water dissolution behavior of the unmodified and Ti-modified MCM-41. In this section, the results of the characterization studies carried out before and after the hydrothermal stability tests are presented.

Before Hydrothermal Stability Tests

XRD diffraction patterns of unmodified MCM-41 and titanium-modified MCM-41 before the hydrothermal stability test are given in Figure 2.
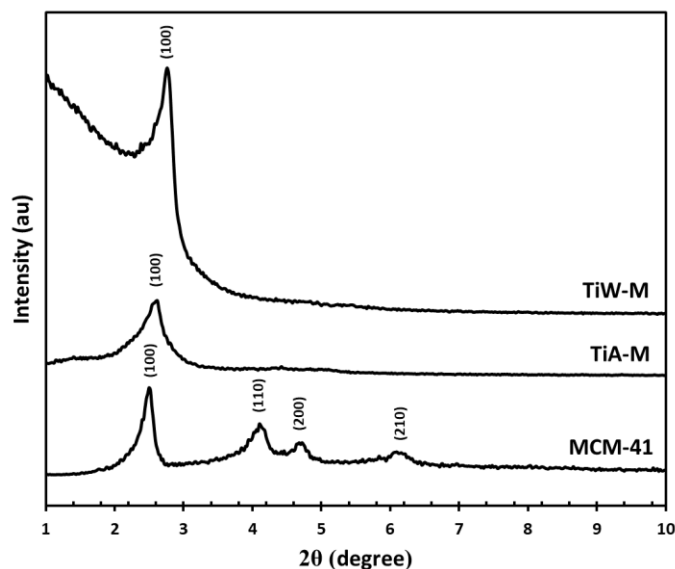
Figure 2. *XRD Patterns of the catalyst supports before the hydrothermal stability test*

The XRD pattern for the unmodified MCM-41 displayed four peak positions (100, 110, 200, and 210 reflections) from 1° to 10°, confirming the typical MCM-41 structure [28]. For the modified MCM-41 with titanium, only the 100 reflection peak was observed, which showed that the hexagonal structure was preserved. In the literature, when metal was added to the MCM-41 structure, the disappearance of the peaks in the (110), (200), and (210) planes indicated that the hexagonal pore structure was preserved despite the disordered structure [29]. Additionally, it was observed that the detected peak shifted to a higher 2θ when titanium was loaded into the MCM-41 structure. This decrease in interplanar d100 spacing resulted from incorporating Ti atoms rather than Si atoms into the MCM-41 structure. The low peak intensity seen for the TiA-M sample indicated the formation of a lamellar phase, which was thought to cross-link and then transform the hexagonal phase [30].

N_2 adsorption/desorption analyses were carried out for unmodified MCM-41 and modified MCM-41 supports. The N_2 adsorption/desorption isotherms and pore size distribution are shown in Figure 3. Structural properties determined from physical adsorption and XRD data are given in Table 1.

Figure 3. N_2 adsorption/desorption isotherms and pore size distributions for the TiW-M and TiA-M support materials.
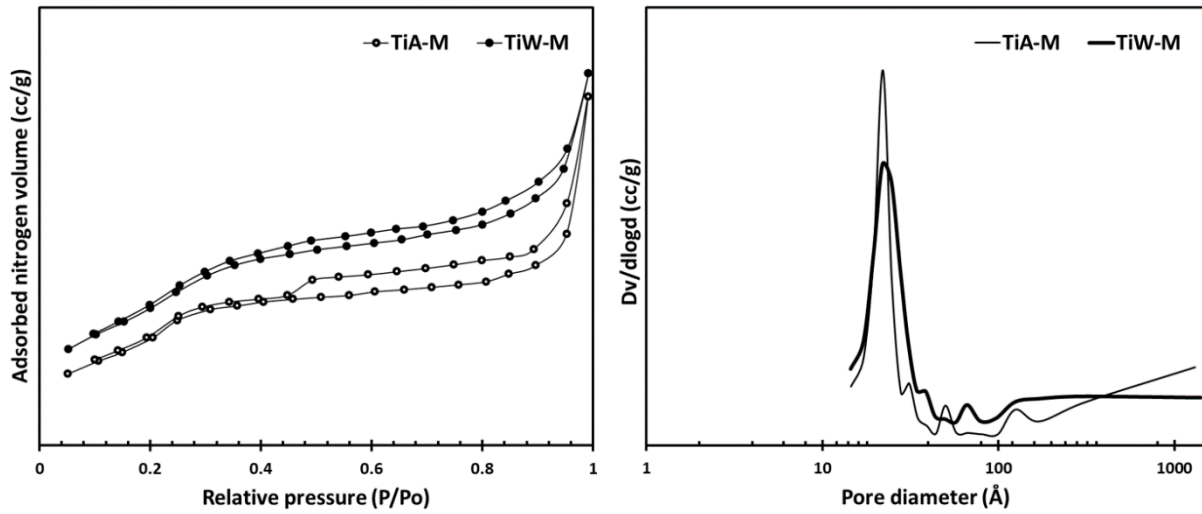
Figure 3. N_2 *adsorption/desorption isotherms and pore size distributions for the TiW-M and TiA-M support materials*

Table 1. *Structural properties of the support materials*

Sample	d, Å	δ, Å	L, Å	Surface area (BET) m²/g	Pore volume cc/g	Pore diameter Å
MCM-41	28	13	-	1250	1.20	28
TiW-M	32	15	178	554	0.59	22
TiA-M	34	18	204	473	0.57	22

d: distance between layers   δ: wall thickness   L: crystal size

It can be seen that both TiW-M and TiA-M samples exhibited typical MCM-41 isotherm characteristics, classified as Type IV and Hysteresis I according to IUPAC classification. Type IV isotherm confirmed the presence of the mesoporous structure, while Hysteresis I indicated a regular and homogeneous formed structure with narrow pore sizes [31]. The absence of a step increase in volume at low relative pressure indicated no microspores in the modified material. Monolayer adsorption of nitrogen molecules occurred on the surface at low relative pressure values (P/Po < 0.2). As relative pressure increased, hysteresis formation and increased adsorption volume after 0.1 (P/Po) showed capillary condensation inside the mesoporous. At close-to-saturation, relative pressure (approaching 1), mesoporous were fully saturated,

while macrospores were partially saturated [32]. Meanwhile, for the TiA-M sample, the existence of ink-bottle pores can be discarded since the desorption branch showed a gentle decrease in the P/Po around 0.45–0.5. BJH adsorption pore size distribution was used to determine the pore diameter of prepared materials. The average mesoporous diameter of TiA-M was found to be identical to TiW-M, measuring 22 Å. It was observed that the surface area and pore volume of the titanium-modified supports decreased when compared to the unmodified MCM-41. This case can be explained by the presence of highly dispersed titanium species blocking the pores of the structure. The pore diameter for MCM-41 (28 Å) was still within the range generally observed for the MCM-41 material [28].

As a result of the data obtained from XRD and N_2 adsorption/desorption analysis, there was no significant difference in the structural and physical properties of the modified MCM-41 samples. A decrease in band gap energy was observed with titanium loading due to an increase in TiO_2 crystal size. Therefore, small crystal sizes were preferred in the literature [33]. The small crystal size may be attributed to the higher surface area, which prevents agglomeration of particles and leads to uniform dispersion of titanium oxide crystals. For this reason, it was decided to use the TiW-M sample with a smaller crystal size and higher surface area in catalyst preparation. FT-IR analyses of the TiW-M support were conducted, and the obtained spectrum is given in Figure 4.
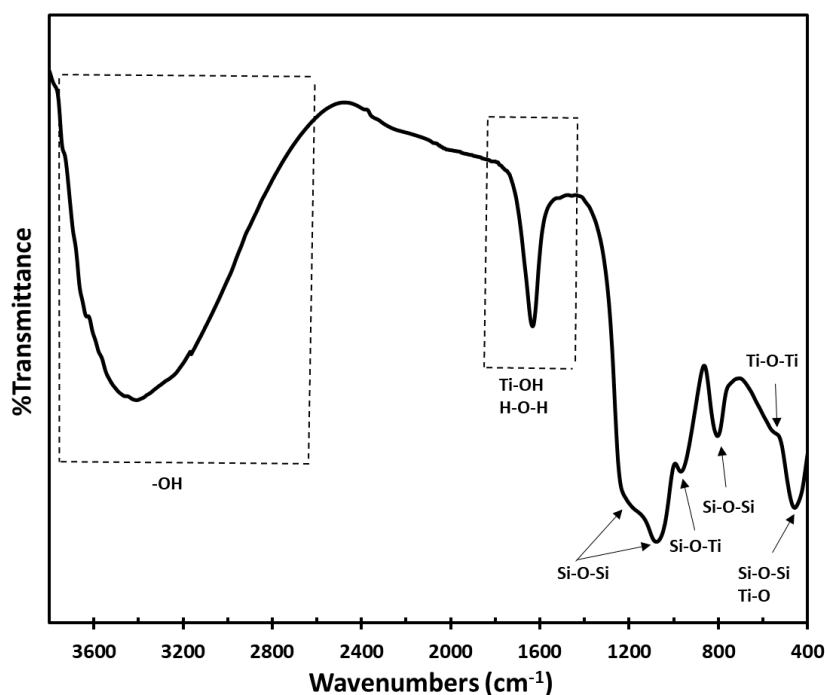
Figure 4. FT-IR spectra of Ti-modified MCM-41

The 3440 cm^{-1} band is associated with the presence of hydroxyl groups (-OH) on the framework. The band at a range of 1645 cm^{-1} corresponds to bending vibrations of the Ti-OH and H-O-H. The band within the 1000–1245 cm^{-1} range is assigned to the presence of Si–O–Si bonds, which are inherent to the siliceous structure and serve as a distinctive characteristic. The band at 800 cm^{-1} is also related to the bending vibrations of the Si–O–Si groups. The presence of the 960 cm^{-1} band in the materials is associated with the isomorphic substitution of Si by Ti ions and is attributed to the stresses of the Si–O–Ti polar bonds [30], [34]. The absorption peak at 690 cm^{-1} is associated with the infrared vibrations of Ti-O in the anatase phase [35]. The bands at 455 cm^{-1} are ascribed to the bending vibrations of the Si–O–Si groups and Ti-O metal oxides.

After Hydrothermal Stability Tests

MCM-41 supports were modified with titanium to increase hydrothermal stability. The XRD patterns of the prepared supports after the hydrothermal stability test are presented in Figure 5.
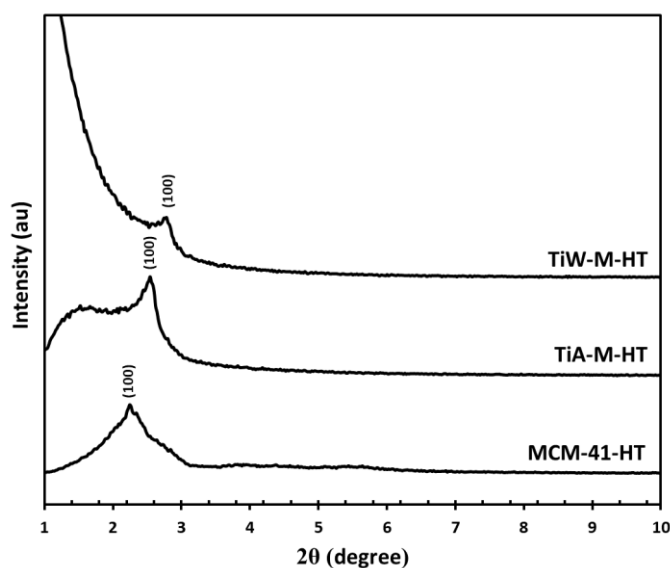

Figure 5. *XRD Patterns of the supports after the hydrothermal stability test*

When Figure 2 and Figure 5 are compared, it can be seen that MCM-41 material shows a structural change after the hydrothermal stability test. According to sample dissolution data, unmodified MCM-41 dissolved in water approximately 9 times more than the Ti-modified support.

XRD patterns revealed structural changes, reducing the main 100-reflection peak intensity for all MCM-41-supported materials after hydrothermal treatment. Unmodified MCM-41 lost the 110, 200, and 210 reflection peaks at 383K. This observation agreed with the literature [36]. The observed structural changes and dissolution data differences between unmodified MCM-41 and titanium-modified MCM-41 after hydrothermal treatment at 383K can be explained based on the inherent bonds in each material and their interactions with water.

MCM-41 contains Si-O-Si bonds in its framework, forming a highly ordered mesoporous structure that can collapse under hydrothermal conditions. In contrast, titanium-modified MCM-41 includes Ti-O-Si bonds resulting from the incorporation of titanium. These bonds are believed to enhance structural stability due to the strong nature of Ti-O bonds. The formation of the Si-O-Ti bond is suggested to have an impact on the prevention of sinterization [37]. Considering water-surface interactions, the hydrothermal exposure of MCM-41 resulted in a significant increase in water adsorption, which was mostly attributed to the presence of Silanol (Si-OH) groups that caused structural damage as water molecules interacted with surface hydroxyl groups. On the other hand, in titanium-modified MCM-41, the presence of Ti-OH and Ti-O-Si bonds probably influenced water adsorption dynamics. The interaction mechanism of Ti-OH with water was different from that of Si-OH, affecting the extent of structural changes. Liu et al. [36] stated that the water adsorption in MCM-41 material shifts from surface adsorption to multilayer adsorption. Also, due to hydrogen bonding, droplets are formed, and capillary condensation further occurs in the pores. Titanium can form strong bonds with oxygen atoms, creating Ti-OH and Ti-O bonds. These bonds contribute to the stabilization of the material's structure, making it more resistant to structural changes even in the presence of water at elevated temperatures [38]. Ti-O bonds tend to be stronger than Si-O bonds, which might contribute to the hydrothermal stability observed in modified MCM-41. It was shown by FT-IR analysis that Ti-OH, Ti-O, and Si-O-Ti bonds, the advantages of which were described in the literature, were present in the prepared support (Figure 4). Consistent with the literature, the hydrothermal stability of the Ti-modified support can be explained by the presence of these bonds.

3.2 Characterization Studies of Chromium-Based Catalysts

In the preparation of chromium-based catalysts, support (TiW-M), which was determined to have a smaller crystal size and higher surface area, was used. The XRD patterns of the synthesized catalysts supported on titanium-doped MCM-41 with different chromium loading (3% and 10% by mass) synthesized by impregnation methods are presented in Figure 6.
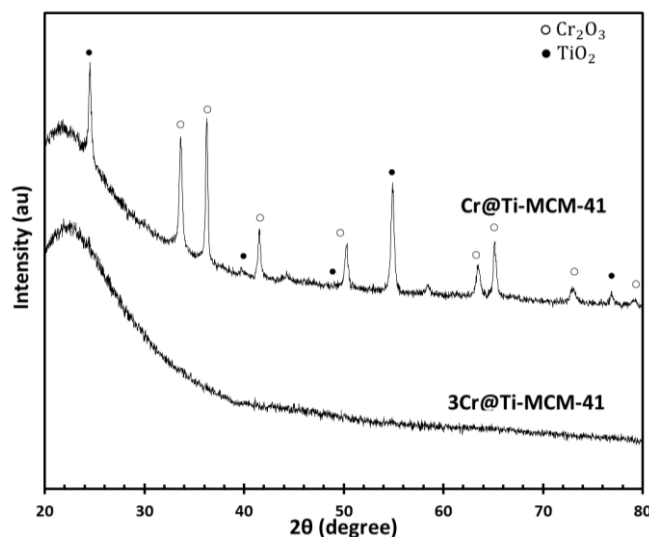
Figure 6. XRD Patterns of Chromium-based Catalysts.

For 3Cr@Ti-MCM-41, a wider peak was observed at 22°, a distinctive feature of the amorphous silica structure. No peaks corresponding to chromium oxide were observed corresponding to the lower chromium content; this could indicate that these particles, if exist, were in an amorphous state or clusters/particles too small to be detected by XRD. As proven by the XRD results in Figure 6, nine peaks (at 2θ: 33.57°, 36.19°, 41.50°, 50.23°, 58.46°, 63.43°, 65.09°, 72.79°, and 79.10°) are observed in the pattern of 10Cr@Ti-MCM-41, which indexed to crystal rhombohedral α-Cr_2O_3 phase (JCPDS 00-006-0504). Also, from the reference patterns, the peaks at 2θ: 24.45°, 39.62°, 54.81°, and 76.83° indexed the TiO_2 anatase phase (JCPDS No.21‑1272). The structural properties of the catalysts are given in Table 2.

Table 2. Structural properties of the prepared catalysts

Catalyst	d(Å)	L (Å) Cr	L (Å) Ti	Surface area (BET) m^2/g
3Cr@Ti-MCM-41	3.90	9.40	-	440
10Cr@Ti-MCM-41	2.70	259	278	352
d: distance between layers		δ: wall thickness		L: crystal size

No significant change was observed in the surface area values of the synthesized catalysts.

SEM/EDS analysis was carried out on synthesized chromium-based catalysts to determine catalyst morphology and composition. SEM photographs are given in Figure 7.
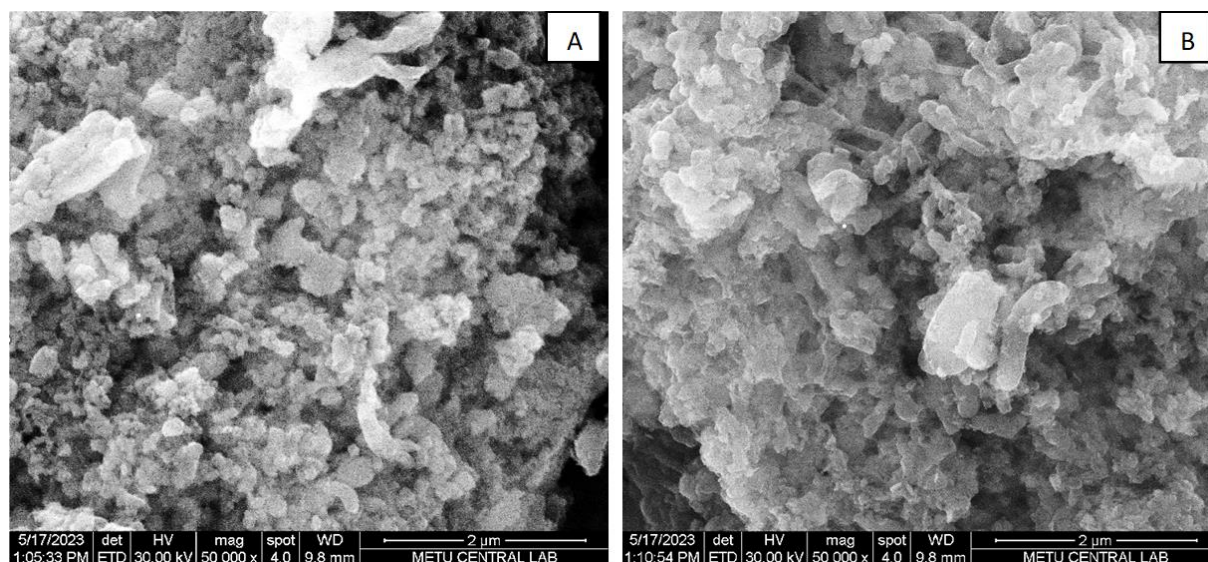
Figure 7.SEM photographs of the catalysts:3Cr@Ti-MCM-41 (A),10Cr@Ti-MCM-41 (B)

SEM images in Figure 7 confirm the homogeneous structure of the catalysts, the highly ordered structure of the MCM-41 support and the surface with a smooth appearance. It was shown that the incorporation of the metal oxides into the mesoporous was successful. Additionally, it was observed that catalysts containing 10% Cr by mass exhibited larger pores. Surface compositions of the chromium-based catalysts by EDS analysis are listed in Table 3.

Table 3. Surface compositions of the chromium-based catalysts

Element Catalyst	Oxygen (O)	Sodium (Na)	Silica (Si)	Potassium (K)	Titanium (Ti)	Chromium (Cr)	Cr/Ti (mass/mass)
3Cr@Ti-MCM-41	58.39	1.31	35.10	0.46	2.18	2.56	1.17
10Cr@Ti-MCM-41	56.52	0.75	32.73	0.69	1.73	7.59	4.38

The amounts of chromium with EDS analysis were predicted as 2.56 and 7.59 (%, by mass), respectively, for 3Cr@Ti-MCM-41 and 10Cr@Ti-MCM-41. Lower chromium amounts were determined by EDS analysis than the chromium amounts (3%

Cr and 10% Cr, by mass) adjusted in the synthesis. This can be explained by the inability to detect chromium embedded in the pore walls of the support by EDS analysis. Similar results were reported in many studies in the literature [3], [39]. Cr/Ti ratios in the synthesis for 3% Cr and 10% Cr were 1.2 and 4, respectively. It can be seen that the Cr/Ti ratios determined from EDS and adjusted in the synthesis were very close to each other.

The 3Cr@MCM-41 catalyst containing 3% chromium by mass was also prepared using unmodified MCM-41 based on the same synthesis procedure. From XRD analysis Cr@MCM-41, the distances between layers (d) and the crystal size (L) were determined as 3.5 Å and 7.3 Å, respectively. from XRD analysis. The surface area (BET) of Cr@MCM-41 was obtained as 400 m^2/g from N_2 adsorption/desorption data.

3.3. Catalytic Tests

Oxidative dehydrogenation of isobutane in the presence of carbon dioxide was conducted over 3Cr@Ti-MCM-41 and 3Cr@MCM-41 catalysts. Isobutane conversion and isobutene selectivity values are shown in Figure 8 and Figure 9, respectively.
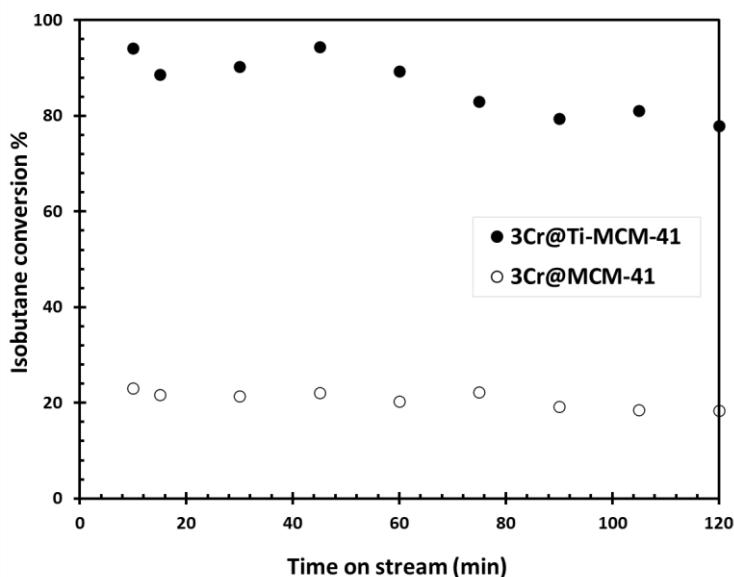
Figure 8. Isobutane conversion values (isobutane/CO$_2$ feed ratio: 1/5, 600 ℃, WHSV: 51 h^{-1})

Figure 9. *Isobutene selectivity values (isobutane/CO_2 feed ratio: 1/5, 600 °C, WHSV: 51 h^{-1})*

As can be seen from Figure 8, isobutane conversion values obtained for 3Cr@Ti-MCM-41 are significantly higher (about 4 times) than that of the 3Cr@MCM-4 catalyst. It was emphasized in section 3.1 that the structural properties (such as surface area value and crystal size) of the 3Cr@Ti-MCM-41 and 3Cr@MCM-41 catalysts were similar. The high difference between the conversions can be explained by the modification of the support. The equilibrium conversion (Gaseq Program) was determined to be 46% at 600°C for a feed ratio of isobutane to CO_2 of 1 to 5 (mol). It can be seen that the conversion values over the 3Cr@MCM-4 catalyst were 50% less than the equilibrium conversion, while the conversion over 3Cr@Ti-MCM-41 exceeded the equilibrium conversion.

A recent study confirmed that the loading of titanium improved catalyst stability when compared to titanium-free catalysts [26]. It was established that doping Ti to MCM-41 significantly modified the structural properties and decreased hydrophobicity. According to the literature, three possible mechanisms can cause a reduction in hydrophobicity when titanium is added. These mechanisms are surface functionalization, surface charge modification, and structural rearrangement [30], [37]. Titanium species bond with Silanol groups (Si-OH) on MCM-41's surface. This case forms hydrophilic groups (like Ti-OH and Ti-O) that interact with water molecules through hydrogen bonding and reduce surface hydrophobicity. The existence of the hydrophilic groups was demonstrated by FT-IR analyses (Figure 4).

It was thought that the presence of hydrophilic groups helped the adsorption of water produced from the oxidative dehydrogenation reaction (Eq. 3).

$$i\text{-}C_4H_{10} + CO_2 \leftrightarrow i\text{-}C_4H_8 + H_2O + CO \qquad \textbf{(3)}$$
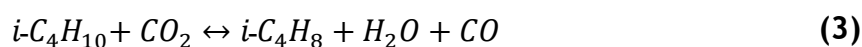
The activity of chromium-based catalysts in dehydrogenation reactions is significantly affected by the number of mono-chromates in the structure [40]. It was reported that the transformation of di-chromates (Eq.4) to monochromates during the reaction occurred in the presence of water [39].

$$H_2O + Cr_2O_7^{2-} \leftrightarrow 2CrO_4^{2-} + 2H^+ \qquad \textbf{(4)}$$
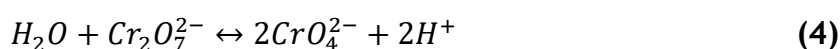
It can be said that the reason for the high conversion values over 3Cr@Ti-MCM-41 catalysts is the higher hydrophilicity achieved by loading Ti. When the selectivity values shown in Figure 9 are examined, it is seen that the 3Cr@Ti-MCM-41 catalyst have the higher selectivity values (60-81%). The appearance of propane, propene, and methane at the reactor outlet during the reaction showed that the following side reactions (Eq. 5 and Eq. 6) took place in both catalysts, more in the 3Cr@MCM-41 catalyst.

$$i\text{-}C_4H_{10} \leftrightarrow C_3H_6 + CH_4 \qquad \textbf{(5)}$$

$$i\text{-}C_4H_{10} + H_2 \leftrightarrow C_3H_8 + CH_4 \qquad \textbf{(6)}$$
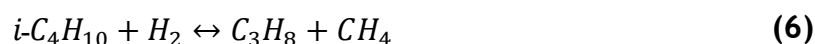
4   CONCLUSIONS

New chromium-based catalysts supported on titanium-modified MCM-41 were synthesized by the impregnation method for oxidative dehydrogenation of isobutane. Hydrothermal stability tests showed that modified MCM-41 resisted structural changes even in the presence of water at high temperatures, unlike unmodified MCM-41. The hydrothermal stability provided by the addition of titanium was explained by the formation of Ti-O-Si, Ti-O, and Ti-OH bonds that strengthened the structure. The interactions between these bonds and water molecules influenced water adsorption behavior. MCM-41 maintained its hexagonal structure even after adding

chromium and titanium into the mesoporous structure. The inactive α-Cr_2O_3 form for the reaction was observed at high Cr-loading. The catalytic tests showed that chromium-based catalysts supported on titanium-modified-MCM-41 exhibited much higher conversion and selectivity values than the catalyst supported on unmodified MCM-41. This case was explained by the improved hydrophilic properties. Hydrophilic groups (Ti-OH and Ti-O) interacted with water molecules through hydrogen bonding and reduced surface hydrophobicity. The most active chromate type in chromium-based catalysts used in oxidative dehydrogenation reactions is monochromates. As the reaction progressed, monochromates turned into dichromates. It was thought that with the help of water adsorbed on the surface, dichromates turned into active monochromates again for catalysts supported on Ti-MCM-41. It can be said that the synthesized new catalyst is a good candidate that can be used in oxidative dehydrogenation reactions with its good hydrothermal stability, suitable textural properties and catalytic properties.

Conflict of Interest

There is no conflict of interest between the authors.

Authors Contributions

Hiba Mustafa Yousef Mosa: Collected the data. Performed the analysis.

Meltem Dogan: Conceived and design the analysis. Wrote the paper.

Saliha Cetinyokus: Contributed data or analysis tools.

Acknowledgment and Support

Statement of Research and Publication Ethics

The study is complied with research and publication ethics.

REFERENCES

[1]   S. Çetinyokuş, M. Doğan and Z. Erol, "Investigation of the effectiveness of Cr@MCM-41 catalysts in isobutane dehydrogenation," *Journal of the Faculty of Engineering and Architecture of Gazi University*, vol. 36, no. 2, pp. 1075-1088, 2021.

[2]   Y. Chen, J. Lyu, Y. Wang, T. Chen and Y. Tian, "Synthesis, characterization, adsorption, and isotopic separation studies of pyrocatechol-modified MCM-41 for efficient boron removal," *Industrial & Engineering Chemistry Research*, vol. 58, no. 8, pp. 3282-3292, Feb. 2019, doi: 10.1021/acs.iecr.8b04748.

[3]   T.H. Liou, S.M. Liu and G.W. Chen, "Utilization of e-wastes as a sustainable silica source in synthesis of ordered mesostructured titania nanocomposites with high adsorption and photoactivity," J*ournal of Environmental Chemical Engineering*, vol. 10, no. 2, 2022, doi: 10.1016/j.jece.2022.107283.

[4]   W.Y. Sang and O.P. Ching, "Tailoring MCM-41 mesoporous silica particles through modified sol-gel process for gas separation," in AIP Conference Proceedings, 2017, vol. 1891, no. 1: AIP Publishing.

[5]   B. Szczesniak, J. Choma and M. Jaroniec, "Major advances in the development of ordered mesoporous materials," *Chemical Communications*, vol. 56, no. 57, pp. 7836-7848, Jul. 2020, doi: 10.1039/d0cc02840a.

[6]   C.S. Ha, S.S. Park, C.S. Ha, and S.S. Park, "General synthesis and physico-chemical properties of mesoporous materials," Periodic Mesoporous Organosilicas: Preparation, Properties and Applications, pp. 15-85, 2019

[7]   S. C. Buratto, E. Latocheski, D.C.D. Oliveira and J. B. Domingos, "Influence of the capping agent PVP of the outer layer of Pd nanocubes surface on the catalytic hydrogenation of unsaturated C– C bonds," *Journal of the Brazilian Chemical Society*, vol. 31, pp. 1078-1085, 2020.

[8]   I. Safo and M. Oezaslan, "Electrochemical cleaning of polyvinylpyrrolidone-capped Pt nanocubes for the oxygen reduction reaction," *Electrochimica Acta*, vol. 241, pp. 544-552, 2017.

[9]   R.Y. Zhong, K.Q. Sun, Y.C. Hong and B.Q. Xu, "Impacts of organic stabilizers on catalysis of Au nanoparticles from colloidal preparation," *Acs Catalysis*, vol. 4, no. 11, pp. 3982-3993, 2014.

[10]   C. Prossl, M. Kubler, M.A. Nowroozi, S. Paul, O. Clemens and U. I. Kramm, "Investigation of the thermal removal steps of capping agents in the synthesis of bimetallic iridium-based catalysts for the ethanol oxidation reaction," *Phys Chem Chem Phys*, vol. 23, no. 1, pp. 563-573, Jan 6 2021, doi: 10.1039/d0cp04900j.

[11]   D.M. Bezerra, I.W. Zapelini, K.N. Franke, M.E. Ribeiro and D. Cardoso, "Investigation of the structural order and stability of mesoporous silicas under a

humid atmosphere," *Materials Characterization*, vol. 154, pp. 103-115, 2019, doi: 10.1016/j.matchar.2019.05.032.

[12]   L. López Pérez, E. R. H. van Eck and I. Melián-Cabrera, "On the hydrothermal stability of MCM-41. Evidence of capillary tension-induced effects," *Microporous and Mesoporous Materials*, vol. 220, pp. 88-98, 2016, doi: 10.1016/j.micromeso.2015.08.024.

[13]   A. Ghasemi and H. Sanaeishoar, "An Efficient one-pot synthesis of 1H-Pyrazolo [1, 2-b] phthalazine-5, 10-dione derivatives using MCM-41," J*ournal of Chemical Reactivity and Synthesis*, vol. 9, no. 3, pp. 58-64, 2019.

[14]   A. Ahmad, M. H. Razali, K. Kassim and K.A.M. Amin, "Synthesis of multiwalled carbon nanotubes supported on M/MCM-41 (M= Ni, Co and Fe) mesoporous catalyst by chemical vapour deposition method," *Journal of Porous Materials*, vol. 25, pp. 433-441, 2018.

[15]   R. De Clercq , M. Dusselier, C. Poleunis, D.P. Debecker, L. Giebeler, S. Oswald, E. Makshina and B.F. Sels, "Titania-silica catalysts for lactide production from renewable alkyl lactates: structure–activity relations," *ACS Catalysis*, vol. 8, no. 9, pp. 8130-8139, 2018, doi: 10.1021/acscatal.8b02216.

[16]   A. S. Al-Awadi, A.M. Toni, M. Alhoshan, A. Khan, J.P. Labis, A. Al-Fatesh, A. E. Abasaeed and S.M. Al-Zahrani, "Impact of precursor sequence of addition for one-pot synthesis of Cr-MCM-41 catalyst nanoparticles to enhance ethane oxidative dehydrogenation with carbon dioxide," (in English), *Ceramics International*, vol. 45, no. 1, pp. 1125-1134, Jan 2019, doi: 10.1016/j.ceramint.2018.10.002.

[17]   Q. Sun, N. Wang and J. Yu, "Advances in catalytic applications of zeolite-supported metal catalysts," *Advanced Materials*, vol. 33, no. 51, p. e2104442, Dec 2021, doi: 10.1002/adma.202104442.

[18]   A. Wróblewska, M. Kujbida, G. Lewandowski, A. Kamińska, Z. C. Koren and B. Michalkiewicz, "Epoxidation of 1, 5, 9-Cyclododecatriene with hydrogen peroxide over Ti-MCM-41 Catalyst," *Catalysts*, vol. 11, no. 11, p. 1402, 2021.

[19]   H. Sekkiou, R. Hamacha, T. Ali-Dahmane, A. Morsli and A. Bengueddach, "The effect of the method of copper incorporation on the structure of Si-MCM-41 and Al-MCM-41," J*ournal de la Société Chimique de Tunisie*, vol. 15, pp. 93-99, 2013.

[20]   P.H. Chao, W.C. C. Jean, H.-P. Lin and T.C. Tsai, "Intercalation of silanes by ion imprinting method for improving hydrothermal stability of mesoporous silica," *Catalysis Today*, vol. 212, pp. 175-179, 2013/09/01/ 2013, doi: 10.1016/j.cattod.2012.08.029.

[21]   M. Song, C. Zou, G. Niu and D. Zhao, "Improving the hydrothermal stability of mesoporous silica SBA-15 by pre-treatment with $(NH_4)_2SiF_6$," *Chinese Journal of Catalysis*, vol. 33, no. 1, pp. 140-151, 2012/01/01/ 2012, doi: 10.1016/s1872-2067(10)60283-5.

[22]   C. Jiang, A. Su, X. Li, T. Zhou and D. He, "Study on the hydrothermal stability of MCM-41 via secondary restructure," *Powder Technology*, vol. 221, pp. 371-374, 2012, doi: 10.1016/j.powtec.2012.01.028.

[23]   Y. Luo, C. Miao, Y. Yue, W. Yang, W. Hua and Z. Gao, "Chromium oxide supported on silicalite-1 zeolite as a novel efficient catalyst for dehydrogenation of isobutane assisted by CO_2," *Catalysts*, vol. 9, no. 12, 2019, doi: 10.3390/catal9121040.

[24]   Y. Luo, C. Wei, C. Miao, Y. Yue, W. Hua and Z. Gao, "Isobutane dehydrogenation assisted by CO_2 over silicalite-1-supported ZnO Catalysts: Influence of Support Crystallite Size," *Chinese Journal of Chemistry*, vol. 38, no. 7, pp. 703-708, 2020, doi: 10.1002/cjoc.202000042.

[25]   A. S. Al-Awadi, A.M. El-Toni, S.M. Al-Zahrani, A.E. Abasaeed, M. Alhoshan, A. Khan, J.P. Labis and A. Al-Fatesh, "Role of TiO_2 nanoparticle modification of Cr/MCM41 catalyst to enhance Cr-support interaction for oxidative dehydrogenation of ethane with carbon dioxide," *Applied Catalysis A: General*, vol. 584, 2019, doi: 10.1016/j.apcata.2019.117114.

[26]   T. Wan, F. Jin, X. Cheng, J. Gong, C. Wang, G. Wu and A. Liu, "Influence of hydrophilicity and titanium species on activity and stability of Cr/MWW zeolite catalysts for dehydrogenation of ethane with CO_2," *Applied Catalysis A: General*, vol. 637, 2022, doi: 10.1016/j.apcata.2022.118542.

[27]   V. Elías, E. Sabre, K. Sapag, S. Casuscelli and G. Eimer, "Influence of the Cr loading in Cr/MCM-41 and TiO_2/Cr/MCM-41 molecular sieves for the photodegradation of Acid Orange 7," A*pplied Catalysis A: General*, vol. 413-414, pp. 280-291, 2012, doi: 10.1016/j.apcata.2011.11.019.

[28]   S. Kilicarslan, M. Dogan and T. Dogu, "Cr incorporated MCM-41 type catalysts for isobutane dehydrogenation and deactivation mechanism," *Industrial & Engineering Chemistry Research*, vol. 52, no. 10, pp. 3674-3682, 2013, doi: 10.1021/ie302543c.

[29]   R. S. Araújo, F. O. S. Costa, D. A. S. Maia, H. B. S. Ana and C. L. Cavalcante, "Synthesis and characterization of Al-and Ti-MCM-41 materials : Application To Oxidation Of Anthracene," 2007.

[30]   A. Wróblewska, P. Miądlicki, J. Tołpa, J. Sreńscek-Nazzal, Z. C. Koren and B. Michalkiewicz, "Influence of the titanium content in the Ti-MCM-41 catalyst on the course of the α-pinene isomerization process," *Catalysts*, vol. 9, no. 5, p. 396, 2019.

[31]   K. Sing, F. Schüth and T. Weitkamp, "Handbook of porous solids," Wiley, vol. 3, pp. 1543-1591, 2002.

[32]   F.J. Sotomayor, K.A. Cychosz and M. Thommes, "Characterization of micro/mesoporous materials by physisorption: concepts and case studies," A*cc. Mater. Surf. Res*, vol. 3, no. 2, pp. 34-50, 2018.

[33]   P. S. Niphadkar, S. K. Chitale, S. K. Sonar, S. S. Deshpande, P. N. Joshi and S. V. Awate, "Synthesis, characterization and photocatalytic behavior of TiO_2–SiO_2 mesoporous composites in hydrogen generation from water splitting," *Journal of Materials Science*, vol. 49, no. 18, pp. 6383-6391, 2014, doi: 10.1007/s10853-014-8365-2.

[34]   S. K. Roy, D. Dutta and A. K. Talukdar, "Highly effective methylated Ti MCM-41 catalyst for cyclohexene oxidation," (in English), *Materials Research Bulletin*, vol. 103, pp. 38-46, Jul 2018, doi: 10.1016/j.materresbull.2018.03.017.

[35]   A. Talati, M. Haghighi and F. Rahmani, "Impregnation vs. coprecipitation dispersion of Cr over TiO_2 and ZrO_2 used as active and stable nanocatalysts in oxidative dehydrogenation of ethane to ethylene by carbon dioxide," *RSC Advances*, vol. 6, no. 50, pp. 44195-44204, 2016, doi: 10.1039/c6ra05049b.

[36]   Y. Liu, Y. Liu, A. Peyrav, Z. Hashisho, S. Zheng, Z. Sun, X. Chen, Y. Tong, Y. Hao and J. Wang, "Experimental and simulation investigation of water vapor adsorption on mesoporous MCM-41 derived from natural Opoka," (in English), *Separation and Purification Technology*, vol. 309, p. 123056, Mar 15 2023, doi: 10.1016/j.seppur.2022.123056.

[37]   C. Gaidau, A. Petica, M. Ignat, L. M. Popescu, R.M. Piticescu, I.A. Tudor and R.R. Piticescu, "Preparation of silica doped titania nanoparticles with thermal stability and photocatalytic properties and their application for leather surface functionalization," (in English), *Arabian Journal of Chemistry*, vol. 10, no. 7, pp. 985-1000, Nov 2017, doi: 10.1016/j.arabjc.2016.09.002.

[38]   K. Bourikas, C. Kordulis and A. Lycourghiotis, "Titanium dioxide (anatase and rutile): surface chemistry, liquid-solid interface chemistry, and scientific synthesis of supported catalysts," *Chem Rev*, vol. 114, no. 19, pp. 9754-823, Oct 8 2014, doi: 10.1021/cr300230q.

[39]   A.D. Erdali, S. Cetinyokus and M. Dogan, "Investigation of isobutane dehydrogenation on $CrOx$/Al_2O_3 catalyst in a membrane reactor," *Chemical Engineering and Processing - Process Intensification*, vol. 175, p. 108904, May 1 2022, doi: 10.1016/j.cep.2022.108904.

[40]   T. Ehiro, A. Itagaki, H. Misu, M. Kurashina, K. Nakagawa, M. Katoh, Y. Katou, W. Ninomiya and S. Sugiyamaet, "Oxidative dehydrogenation of isobutane to isobutene on metal-doped MCM-41 catalysts," *Journal of Chemical Engineering of Japan*, vol. 49, no. 2, pp. 136-143, 2018.

THE PRACTICAL INTEGRATION OF LINEAR ALGEBRA IN GENETICS, CUBIC SPLINE INTERPOLATION, ELECTRIC CIRCUITS AND TRAFFIC FLOW

Khadeejah James Audu [1], * (iD), **Yak Chiben Elisha** [1] (iD), **Yusuph Amuda Yahaya** [2] (iD),
Sikirulai Abolaji Akande[1] (iD)

[1] *Department of Mathematics, Federal University of Technology, Minna, Nigeria,*
k.james@futminna.edu.ng, chiben.m1804731@st.futminna.edu.ng, siqlam@yahoo.com
[2] *Department of Mathematics, Pen Resource University, Gombe, Nigeria, yusuph.yahaya@pru.edu.ng*
* *Corresponding author*

ABSTRACT

A fundamental mathematical field with many applications in science and engineering is linear algebra. This paper investigates the various applications of linear algebra in the fields of traffic flow analysis, electric circuits, cubic spline interpolation, and genetics. This research delves into individual applications while emphasizing cross-disciplinary insights, fostering innovative solutions through the convergence of genetics, cubic spline interpolation, circuits, and traffic flow analysis.

The research employs specific methodologies in each application area to demonstrate the practical integration of linear algebra in genetics, cubic spline interpolation, electric circuits, and traffic flow analysis.

In genetics, linear algebra techniques are utilized to represent genetic data using matrices, analyze genotype distributions across generations, and identify genotype-phenotype associations. For cubic spline interpolation, linear algebra is employed to construct smooth interpolating curves, involving the derivation of equations for spline functions and the determination of coefficients using boundary conditions and continuity requirements. In electric circuit analysis, linear algebra is crucial for modeling circuit elements, formulating systems of linear equations based on Kirchhoff's laws, and solving for voltage and current distributions in circuits. In traffic flow analysis, linear algebra techniques are used to represent traffic movement in networks, formulate systems of linear equations representing traffic flow dynamics, and solve for traffic flow solutions to optimize transportation networks.

By addressing contemporary challenges, emerging research frontiers, and future trajectories at the intersection of linear algebra and diverse domains, this study underscores the profound impact of mathematical tools in advancing understanding and resolving complex real-world problems across multiple fields.

1   INTRODUCTION

This research work delves into the versatile applications of linear algebra in genetics, cubic spline interpolation, electric circuits, and traffic flow analysis. As a foundational mathematical discipline, linear algebra serves as a unifying framework transcending disciplinary boundaries [9]. It plays a pivotal role in genetic data analysis, employing techniques like eigenvalues eigenvectors and diagonalization of matrix [8]. In cubic spline interpolation, linear algebra forms the bedrock, influencing applications in image processing, computer graphics, and motion analysis as demonstrated [10].

This study extends its focus to electric circuits, where linear algebra simplifies simple circuit analysis, fostering efficient design and optimization [2]. Additionally, linear algebra contributes significantly to modelling and analysing traffic flow systems, offering insights into network behaviour, optimization, and control. This research unravels the interconnected contributions of linear algebra across these diverse domains, emphasizing its cross-disciplinary significance and potential to revolutionize problem-solving in genetics, cubic spline interpolation, circuits, and traffic flow analysis [5].

The research identifies a critical gap in existing studies that have individually explored the application of linear algebra in genetics, cubic spline interpolation, electric circuits, and traffic flow. The lack of comprehensive research addressing the synergies and cross-disciplinary implications of employing linear algebra across these diverse domains constitutes a significant research gap. The study aims to bridge this gap by systematically applying linear algebraic principles, offering a unified perspective on the interconnectedness of mathematical principles across these scientific realms. The motivation behind the study lies in the potential to discover novel connections, optimize mathematical models, and improve solutions within each domain, contributing to advancements and fostering interdisciplinary collaboration. The novelty of the research lies in its integrative approach, providing a fresh perspective on problem-solving methodologies and offering new avenues for research and practical applications. Overall, the study is expected to contribute significantly to knowledge by uncovering hidden patterns and relationships, fostering a nuanced understanding of underlying structures.

The literature presents a multifaceted exploration of various research studies. In one instance, [5] underscores the significance of a strategic approach to modeling electrical power systems within communication networks, highlighting diverse methods such as experimental, software-based, and analytical modeling. [6] employs the cubic spline interpolation method to effectively interpolate original noise data, ensuring the seamless connection of noise data for a detailed description and recognition of characteristics within the output layer. In a different context, [1] introduces a cubic spline interpolation algorithm to categorize emotions in speech using curve-fitting techniques, utilizing datasets like Ryerson Audio-Visual Berlin (Emo-DB), Surrey Audio-Visual Expressed Emotion (SAVEE), and Database of Emotional Speech and Song (RAVDESS). Furthermore, [7] delves into the significance of linear algebra methods in solving systems of linear equations, exploring techniques such as scalar augmentation, determinants, and vector space. Each study contributes unique insights and methodologies to their respective fields of research.

The paper presents a comprehensive exploration of the practical integration of linear algebra across genetics, cubic spline interpolation, electric circuits, and traffic flow analysis. In genetics, the research provides a systematic approach for analyzing genotype distributions and identifying genetic markers associated with diseases. For cubic spline interpolation, it offers a methodical process for constructing accurate interpolating curves, enhancing applications in computer graphics and data analysis. In electric circuits, the study advances understanding by demonstrating how linear algebra facilitates the analysis and design of circuits, crucial for electronics and power systems. Moreover, in traffic flow analysis, the research elucidates how linear algebra techniques optimize transportation networks, leading to insights into traffic dynamics and urban planning. Overall, the paper's findings underscore the profound impact of linear algebra in advancing understanding and resolving complex real-world problems across diverse scientific and engineering disciplines, offering valuable contributions to each field.

2 METHODOLOGY

2.1 Genetic Data Representation Using Matrices

The genotype distribution of a particular trait in a population in the *nth* generation can be represented by a genotype vector;

$$P^n = \begin{bmatrix} f_n \\ g_n \\ h_n \end{bmatrix} \tag{1}$$

where f_n, g_n and h_n are the portion with population *AA*, *Aa* and *aa* respectively in the *nth* generation. Since the genotype distribution changes over time, the succession of genotype distributions from one generation to the next will be represented in the form;

$$P^n = TP^{n-1} \tag{2}$$

for a suitable matrix *T* as n = 1,2,3,… an explicit description of P^n whose formula for each P^n does not depend on T or on the preceding terms in the sequence other than the initial term P^0 (the initial genotype distribution in the population),will given as;

$$P^n = TP^{n-1} = T^2 P^{n-2} = ... = T^n P^0 \tag{3}$$

Therefore, the explicit expression for T^n will be obtained by diagonalizing *T*. Hence,

$$T^n = VD^n V^{-1} \tag{4}$$

where *V= Eigenvector* and *D=Diagonal Matrix of T*

Solving for V, D^n and V^{-1}, the obtained outcome becomes

$$D = \begin{bmatrix} \lambda_1 & 0 & 0 \\ 0 & \lambda_2 & 0 \\ 0 & 0 & \lambda_3 \end{bmatrix}, \; V = \begin{bmatrix} 1 & 1 & 1 \\ 0 & -1 & -2 \\ 0 & 0 & 0 \end{bmatrix} \text{ and } V^{-1} = \begin{bmatrix} 1 & 1 & 1 \\ 0 & -1 & -2 \\ 0 & 0 & 1 \end{bmatrix} \tag{5}$$

Substituting (5) in (4), it gives as shown in (Kizilaslan & Acer, 2023);

$$T^n = \begin{bmatrix} \lambda_1 & 0 & 0 \\ 0 & \lambda_2 & 0 \\ 0 & 0 & \lambda_3 \end{bmatrix} \begin{bmatrix} 1 & 1 & 1 \\ 0 & -1 & -2 \\ 0 & 0 & 0 \end{bmatrix} \begin{bmatrix} 1 & 1 & 1 \\ 0 & -1 & -2 \\ 0 & 0 & 1 \end{bmatrix} \tag{6}$$

Putting (6) into (3), the result is

$$P^n = \begin{bmatrix} f_n \\ g_n \\ h_n \end{bmatrix} = \begin{bmatrix} 1 & 1-\left(\frac{1}{2}\right)^n g_0 & 1-\left(\frac{1}{2}\right)^{n-1} h_0 \\ 0 & \left(\frac{1}{2}\right)^n g_0 & \left(\frac{1}{2}\right)^{n-1} h_0 \\ 0 & 0 & 0 \end{bmatrix} \qquad for\, n = 1, 2, 3, \ldots \qquad (7)$$

(7) is the expression for the distribution of the three possible genotypes $\underline{AA}, \underline{Aa}$ and $\underline{aa}$ in the population after any number of generations.

2.1.1 Genetics problem algorithm

Step 1: Define the genetics problem and identify the aspect it relates to.

Step 2: Create a matrix or set of linear equations considering the relevant genetic variables and principles.

Step 3: Collect the necessary genetic information, including genotype/phenotype frequencies and known inheritance patterns.

Step 4: Solve the matrix equation using linear algebraic techniques.

Step 5: Evaluate the outcomes in relation to the genetics puzzle and verify the solution by comparing it with empirical or experimental data.

It is noteworthy that in the Genetics Problem Algorithm (Step 2), the selection of genetic variables and principles is guided by fundamental genetic principles and the specific traits under investigation. This includes considering variables relevant to the traits being studied and applying principles such as Mendelian inheritance and allele frequencies. The rationale for these choices ensures that the resulting matrices accurately represent the genetic dynamics of the problem at hand. By aligning with established genetic principles, the algorithm facilitates the creation of matrices that effectively capture the genetic variation within populations across generations.

2.2 Cubic Spline Representation Using Linear Algebra

The general form of a cubic spline is given as;

$$\underline{S}(x) = \begin{cases} \underline{S}_0(x), x_0 \le x \le x_1 \\ \underline{S}_1(x), x_1 \le x \le x_2 \\ \mathbf{M} \\ \underline{S}_{n-1}(x), x_{n-1} \le x \le x_n \end{cases} \qquad (8)$$

where $\underline{S}_1(x),\ \underline{S}_2(x),...,\ \underline{S}_{n-1}(x)$ are cubic polynomials. For convenience, (6) is written in the form;

$$
\begin{aligned}
\underline{S}_0(x) &= e_0 + f_0(x-x_0) + g_0(x-x_0)^2 + h_0(x-x_0)^3, x_0 \leq x \leq x_1 \\
\underline{S}_1(x) &= e_1 + f_1(x-x_1) + g_1(x-x_1)^2 + h_1(x-x_1)^3, x_1 \leq x \leq x_2 \\
& M \\
\underline{S}_{n-1}(x) &= e_{n-1} + f_{n-1}(x-x_{n-1}) + g_{n-1}(x-x_{n-1})^2 + h_{n-1}(x-x_{n-1})^3, x_{n-1} \leq x \leq x_n
\end{aligned}
\tag{9}
$$

The $e_k{}'s,\ f_k{}'s,\ g_k{}'s$ and $h_k{}'s$ constitute a total of $4n-4$ coefficients that must be determined to specify $\underline{S}(x)$ completely as demonstrated in [1]. If these coefficients are chosen so that $\underline{S}(x)$ interpolates the n specified points in the plane $\underline{S}(x),\ \underline{S}'(x)$ and $\underline{S}''(x)$ are continuous, then the resulting interpolating curve is called a Cubic Spline [3-4]. A cubic spline has four condition and two boundary condition which are used to get the equations required. These conditions are stated below;

1. $\underline{S}(x)$ interpolates the points $(x_k, y_k),\ k = 0,1,...,n$.

2. $\underline{S}(x)$ is continuous on $[x_0, x_n]$.

3. $\underline{S}'(x)$ is continuous on $[x_0, x_n]$

4. $\underline{S}''(x)$ is continuous on $[x_0, x_n]$.

The boundary conditions are;

1. Free/Natural Cubic Spline; $\quad \begin{aligned} \underline{S}_0''(x_0) &= 0 \\ \underline{S}_{n-1}''(x_n) &= 0 \end{aligned}$

2. Clamed/Complete Cubic Spline; $\quad \begin{aligned} \underline{S}_0'(x_0) &= f'(x_0) \\ \underline{S}_{n-1}'(x_n) &= f'(x_n) \end{aligned}$

Applying the four cubic spline conditions on (9) and the boundary conditions, the following equations are obtained;

$$e_0 = y_0$$
$$e_1 = y_1$$
$$\vdots$$
$$e_{n-1} = y_{n-1} \tag{10}$$

$$e_{n-1} + f_{n-1}(x - x_{n-1}) + g_{n-1}(x - x_{n-1})^2 + h_{n-1}(x - x_{n-1})^3 = y_n \tag{11}$$

$$e_0 + f_0(x - x_{n-1}) + g_0(x - x_{n-1})^2 + h_0(x - x_{n-1})^3 = y_1$$
$$e_1 + f_1(x - x_{n-1}) + g_1(x - x_{n-1})^2 + h_1(x - x_{n-1})^3 = y_2$$
$$\mathbf{M}$$
$$e_{n-1} + f_{n-1}(x - x_{n-1}) + g_{n-1}(x - x_{n-1})^2 + h_{n-1}(x - x_{n-1})^3 = y_n \tag{12}$$

$$f_0 + 2g_0(x - x_{n-1}) + 3h_0(x - x_{n-1})^2 = f_1$$
$$f_1 + 2g_1(x - x_{n-1}) + 3h_1(x - x_{n-1})^2 = f_2$$
$$\mathbf{M}$$
$$f_{n-1} + 2g_{n-1}(x - x_{n-1}) + 3h_{n-1}(x - x_{n-1})^2 = f_n \tag{13}$$

$$2g_0 + 6h_0(x - x_{n-1}) = 2g_1$$
$$2g_0 + 6h_0(x - x_{n-1}) = 2g_2$$
$$\vdots$$
$$2g_{n-1} + 6h_{n-1}(x - x_{n-1}) = 2g_n \tag{14}$$

The equations (10), (11), (12), (13), (14) and either the natural cubic spline boundary condition or the clamped cubic spline boundary condition are utilized to constitute a linear system which are then solved by Gauss-Jordan elimination method is used to get the values of the constants in (9) [6].

2.2.1 Cubic spline interpolation algorithm

Step 1: Identify data points for cubic spline interpolation.

Step 2: Calculate the number of intervals between data points.

Step 3: Formulate a system of linear equations.

Step 4: Express the equations as ($Ty = b$).

Step 5: Solve the matrix equation to obtain coefficients for the cubic spline function.

In the Cubic Spline Interpolation Algorithm (Step 1), identifying data points for interpolation involves a thoughtful selection process aimed at capturing the behavior

of the function or dataset accurately. Firstly, data points should ideally be uniformly distributed across the range to ensure comprehensive coverage of the function's behavior. This entails including critical points such as extrema and inflection points, which offer valuable insights into the curve's behavior. However, it's crucial to strike a balance between data sparsity and richness; too few points may lead to inaccuracies, while an excessive number could result in overfitting. Additionally, the quality of data points must be ensured, avoiding inaccuracies or outliers that could compromise the reliability of the interpolation. Context is also vital; data points should align with the specific application's requirements and provide meaningful insights into the problem at hand. By adhering to these guidelines, the selection of suitable data points lays the foundation for an accurate and meaningful interpolation process, facilitating a robust analysis of the function or dataset.

2.3 Matrix Representation of Circuits

Linear algebra stands as a crucial tool in the arsenal of electricians working with electrical circuits. Among the fundamental principles applied in this domain is the use of matrices, particularly in constructing systems of linear equations based on Kirchhoff's voltage law, Kirchhoff's current law, and Ohm's law for simple electrical circuits. While a single permutation suffices to solve equations in straightforward circuits, more intricate circuits demand node analysis. To elucidate, consider the electrical circuit depicted in Figure 1 as an example.
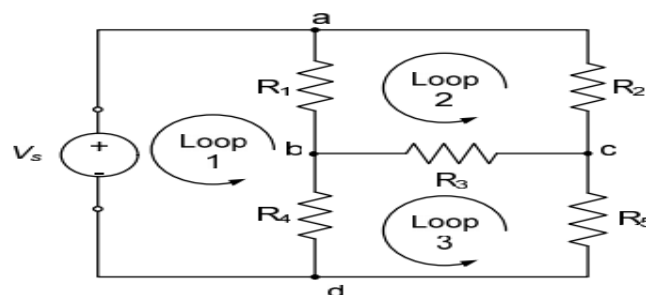
Figure 1. Simple Electric Circuit

Central Concept: Kirchhoff's Voltage Law dictates the flow of current, asserting that the algebraic sum of voltages or voltage drops along any closed path within a network, oriented in a single direction, equals zero. This principle serves as the foundational concept for establishing the system of equations. The resulting system of linear equations follows a specific form due to this fundamental law.

$$RI = V \qquad (15)$$

where R= Resistance (Ohms), I= Current (Ampere) and V= Voltage (Volts). In this scenario, equation (15) signifies the fundamental principle known as Ohm's Law, which relates the current (I) flowing through a resistor to its resistance (R) and the resulting voltage drop (V) across it. Ohm's Law serves as a cornerstone in electrical engineering, establishing a direct relationship between a circuit component's resistance, the current passing through it, and the voltage across it. By applying Ohm's Law, we can predict the behavior of current and voltage in response to variations in resistance or applied voltage, crucial for comprehending and engineering electric circuits. Employing Kirchhoff's voltage law on each loop, the following equations will be constituted;

Loop 1: $I_1 R_4 + I_1 R_1 - I_2 R_1 - I_3 R_4 = -V_s$

$$\left(R_1 + R_4\right) I_1 - I_2 R_1 - I_3 R_4 = -V_s \tag{16}$$

Loop 2: $-I_1 R_1 + I_2 R_1 + I_2 R_2 + I_2 R_3 + I_3 R_3 = 0$

$$-I_1 R_1 + \left(R_1 + R_2 + R_3\right) I_2 + I_3 R_3 = 0 \tag{17}$$

Loop 3: $-I_1 R_4 + I_2 R_3 + I_3 R_3 + I_3 R_4 + I_3 R_5 = 0$

$$-I_1 R_4 + I_2 R_3 + \left(R_3 + R_4 + R_5\right) I_3 = 0 \tag{18}$$

Equations (16), (17), and (18) undergo transformation into a linear system, yielding:

$$\begin{bmatrix} \left(R_1 + R_4\right) & -R_1 & -R_4 \\ -R_1 & \left(R_1 + R_2 + R_3\right) & R_3 \\ -R_1 & R_3 & \left(R_3 + R_4 + R_5\right) \end{bmatrix} \begin{bmatrix} I_1 \\ I_2 \\ I_3 \end{bmatrix} = \begin{bmatrix} -V_s \\ 0 \\ 0 \end{bmatrix}$$

The augmented matrix of the linear system is obtained as;

$$\left[\begin{array}{ccc|c} \left(R_1 + R_4\right) & -R_1 & -R_4 & -V_s \\ -R_1 & \left(R_1 + R_2 + R_3\right) & R_3 & 0 \\ -R_1 & R_3 & \left(R_3 + R_4 + R_5\right) & 0 \end{array}\right]$$

The Gauss-Jordan elimination method is utilized to achieve the reduced-row echelon form of the matrix, which is subsequently employed to obtain the solution for the circuit, as exemplified in [7].

2.3.1 Electric circuit algorithm

Step 1: Describe the electric circuit components and connections.

Step 2: Assign variables to unknown quantities in the circuit.

Step 3: Apply Kirchhoff's laws to formulate equations.

Step 4: Create a system of linear equations representing relationships.

Step 5: Solve the matrix equation using linear algebra techniques to analyze voltages and currents.

In the Electric Circuit Algorithm (Step 1), understanding Kirchhoff's laws is pivotal for analyzing electrical circuits. Kirchhoff's Voltage Law (KVL) dictates that the sum of voltage changes around any closed loop in a circuit equals zero, providing insights into voltage distribution. Similarly, Kirchhoff's Current Law (KCL) states that the total current entering a junction equals the total current leaving, facilitating the analysis of current flow. These laws serve as foundational principles, guiding engineers in formulating equations that represent circuit behavior. By adhering to Kirchhoff's laws, analysts can systematically analyze complex circuits, predict their behavior, and solve for circuit variables using linear algebra techniques. This understanding is crucial for designing, troubleshooting, and optimizing electrical circuits effectively.

2.4 Network Representation of Traffic System

The movement of traffic along the branches is examined to derive systems of linear equations. To establish these equations, an assumption is made that the traffic entering an intersection must exit that intersection, ensuring a balance where the flow into and out of each node is equal. Additionally, it is assumed that the total traffic entering the network equals the total traffic leaving the network, emphasizing the importance of a well-balanced network. To gain a deeper understanding of traffic flow dynamics, Figure 2 is analyzed.
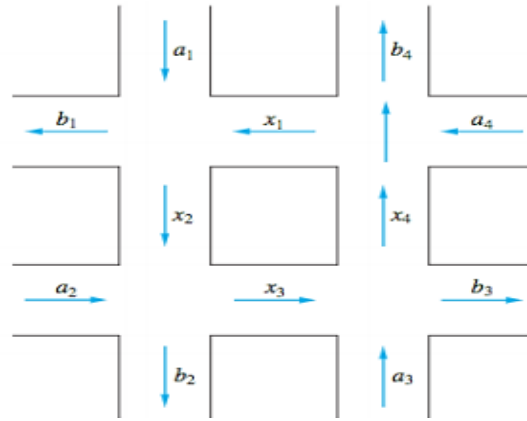
Figure 2. A Traffic Flow Pattern

The system of linear equations will have the form; *Flow In = Flow Out*

At the 1st *Node* ; *Flow In = Flow Out*

$$a_1 + x_1 = b_1 + x_2$$

$$x_1 - x_2 = b_1 - a_1 \qquad (19)$$

At the 2nd *Node* ; *Flow In = Flow Out*

$$x_2 + a_2 = x_3 + b_2$$

$$x_2 - x_3 = b_2 - a_2 \qquad (20)$$

At the 3rd *Node* ; *Flow In = Flow Out*

$$x_3 + a_3 = x_4 + b_3$$

$$x_3 - x_4 = b_3 - a_3 \qquad (21)$$

At the 4th *Node* ; *Flow In = Flow Out*

$$x_4 + a_4 = x_1 + b_4$$

$$x_4 - x_1 = b_4 - a_4 \qquad (22)$$

Using (3.40), (3.41), (3.42) and (3.43) to generate a linear system in the form *Ax=b*;

$$\begin{bmatrix} 1 & -1 & 0 & 0 \\ 0 & 1 & -1 & 0 \\ 0 & 0 & 1 & -1 \\ -1 & 0 & 0 & 1 \end{bmatrix} \begin{bmatrix} x_1 \\ x_2 \\ x_3 \\ x_4 \end{bmatrix} = \begin{bmatrix} b_1 - a_1 \\ b_2 - a_2 \\ b_3 - a_3 \\ b_4 - a_4 \end{bmatrix}$$

The augmented matrix of the linear system is represented as;

$$\begin{bmatrix} 1 & -1 & 0 & 0 & \big| & b_1 - a_1 \\ 0 & 1 & -1 & 0 & \big| & b_2 - a_2 \\ 0 & 0 & 1 & -1 & \big| & b_3 - a_3 \\ -1 & 0 & 0 & 1 & \big| & b_3 - a_3 \end{bmatrix}$$

Utilizing the Gauss-Jordan elimination technique, the reduced-row echelon form of the matrix will be obtained, allowing for the solution of the traffic flow problem.

2.4.1 Traffic flow algorithm

Step 1: Define the traffic flow problem.

Step 2: Gather relevant data on the road network.

Step 3: Formulate the traffic flow problem mathematically.

Step 4: Solve the system of equations using linear algebra techniques.

Step 5: Interpret the mathematical solution to gain insights into traffic flow dynamics.

In the Traffic Flow Algorithm (Step 1), understanding the importance of a balanced network is crucial for effectively modeling traffic dynamics. A balanced network ensures that the flow of traffic into and out of each intersection or node is equal, maintaining equilibrium and efficient traffic movement throughout the network. For example, in a well-balanced network, the total number of vehicles entering an intersection matches the total number exiting, preventing congestion or bottlenecks. This balance is essential for optimizing traffic flow, minimizing delays, and ensuring smooth transportation operations. By considering the significance of network balance, analysts can accurately model traffic flow dynamics, formulate systems of linear equations, and devise effective strategies for traffic management and urban planning. Therefore, ensuring a balanced network is a fundamental aspect of the Traffic Flow Algorithm, facilitating the accurate analysis and optimization of transportation systems.

2.5 Numerical Methods for Linear Systems

Linear algebraic methods, notably Gaussian Elimination and Gauss-Jordan Elimination, play a crucial role in efficiently and accurately finding solutions to problems in various scientific, engineering, and mathematical fields. Gaussian

Elimination systematically transforms linear systems into upper triangular form, facilitating efficient determination of variable values through back substitution. Gauss-Jordan Elimination refines systems into reduced row-echelon form, simplifying solution extraction and providing comprehensive insights into system properties, even in complex scenarios. These methods rely on basic row operations and are fundamental in solving linear systems across diverse domains. In the Traffic Flow Algorithm (Step 1), employing techniques like Gaussian elimination or Gauss-Jordan elimination enhances comprehension and analysis of traffic flow dynamics, streamlining solution processes and optimizing transportation networks effectively. Understanding these numerical methods enhances the Traffic Flow Algorithm's efficacy in traffic flow dynamics analysis and optimization.

3 NUMERICAL ANALYSIS

Experiment 1: In a controlled experimental farm, there exists a substantial population of flowers encompassing all potential genotypes (AA, Aa, and aa) with initial frequencies denoted as $f_0 = 0.05$, $g_0 = 0.90$, and $h_0 = 0.05$. It is assumed that these genotypes determine flower color, and each flower is fertilized by a flower sharing a similar genotype. The task is to derive an expression for the genotype distribution in the population after four generations and to make predictions regarding the long-term genotype distribution after an infinite number of generations.

A concise explanation of the significance of the experiment involves investigating the dynamics of genotype distribution in a flower population across generations. Initially, the population encompasses three genotypes (AA, Aa, and aa) with frequencies $f_0 = 0.05$, $g_0 = 0.90$, and $h_0 = 0.05$, respectively, presumed to determine flower color. Flowers with similar genotypes fertilize each other, and through genetic inheritance principles, the experiment aims to deduce the genotype distribution after four generations. This analysis offers insights into short-term genotype frequency changes and predicts long-term distributions. Understanding such dynamics has practical applications in agriculture and conservation, guiding breeding strategies, preserving genetic diversity, and effectively managing populations, thereby enhancing crop yields, biodiversity preservation, and ecosystem sustainability.

Experiment 2: Employ a linear algebra technique to construct a natural cubic spline that passes through the points (1, 2), (2, 3) and (3, 5).

To accurately interpolate data points and capture the underlying behavior of the dataset in experiment 2, it is imperative to design a natural cubic spline. When piecewise cubic polynomial functions are connected smoothly across data points and function and derivative values remain continuous, the result is a natural cubic spline. Natural cubic splines offer a trustworthy representation of the data by minimizing interpolation mistakes and guaranteeing smoothness and continuity. Due to the ability to precisely approximate data and fit curves, this is advantageous for applications including image processing, computer graphics, and motion analysis. For instance, using the linear algebra approach, in the scenario where the points (1, 2), (2, 3), and (3, 5) are supplied, matrices are created and equations are solved to find the coefficients of the cubic spline that passes through these points.

Experiment 3: Use linear algebra method to determine the three loop currents I_1, I_2 and I_3 in the circuit.
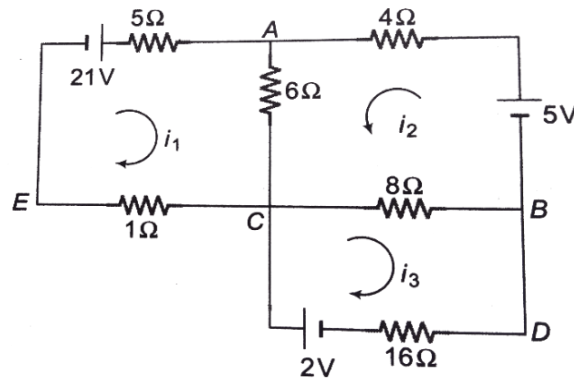
Figure 3. Designed Circuit Problem

Experiment 4: The network in the Figure 4.3 shows the traffic flow (in vehicles per hour) over several one-way street in the downtown area of a certain city during a typical lunch time. Determine the general flow pattern for the network. What is the maximum possible value of x_4?
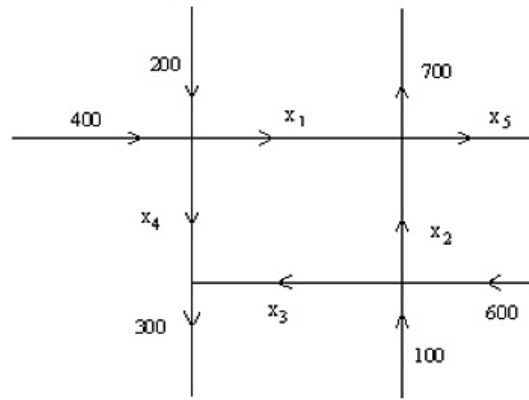
Figure 4. *Traffic Flow Diagram*

The numerical solutions of experiment 1, 2, 3 and 4 are obtained using the algorithms described in (2.1.1), (2.2.1), (2.3.1) and (2.4.1), the results are shown in the tables below.

Table 1. *Computational Result for Experiment 1*

No. of Generation (n)	f_n	g_n	h_n
0	0.05	0.90	0.05
1	0.28	0.45	0.28
2	0.39	0.23	0.39
3	0.44	0.11	0.44
4	0.47	0.06	0.47
∞	0.5	0	0.5

Table 2. *Computational Result of Experiment 2*

Constants	Values
e_0	2
f_0	$\frac{3}{4}$
g_0	0
h_0	$\frac{1}{4}$
e_1	3
f_1	$\frac{3}{2}$
g_1	$\frac{3}{4}$
h_1	$-\frac{1}{4}$

Table 3. *Comparative Result of Experiment 3*

Linear Algebra Method	Iteration	Time (millisecond)
Gaussian Elimination	-	0.00
Gauss-Jordan Elimination	-	0.00
Jacobi	11	1.27
Gauss-Seidel	6	1.17

Table 4. *Computational Result of Experiment 4*

Unknowns	Flow Pattern
x_1	$600 - x_4$
x_2	$400 + x_4$
x_3	$300 - x_4$
x_4	Free
x_5	300

Table 1 shows the expression for the genotype distribution of the population after 4 generation and after an infinite number of generations. In Table 1, the genetic distributions represent the frequencies of different genotypes (AA, Aa, and aa) within a population across multiple generations. As the generations progress from 0 to 4, there are observable changes in the genotype frequencies. Initially, at generation 0, the frequencies are f0 = 0.05, g0 = 0.90, and h0 = 0.05 for genotypes AA, Aa, and aa, respectively. Subsequently, with each generation, there are shifts in these frequencies due to genetic recombination, mutation, selection, and other evolutionary processes. For instance, by generation 4, the frequencies have changed to f4 = 0.47, g4 = 0.06, and h4 = 0.47. These changes in genotype frequencies over generations provide insights into the genetic dynamics of the population, including patterns of inheritance, allele frequencies, and the impact of evolutionary forces. Analyzing these trends provides valuable insights into genetic dynamics, inheritance patterns, and population evolution.

Table 2 presents the computed values of constants necessary for constructing a natural cubic spline in Experiment 2. These constants determine the coefficients of cubic polynomials, ensuring smooth interpolation between specified data points. The table's data facilitates accurate representation of data and curve fitting,

benefiting applications like image processing and motion analysis. The values of the constants have been calculated as depicted in Table 2. Substituting the values of the constants in (9), the natural cubic spline function will now be stated as;

$$\underline{S}_0(x) = 2 + \tfrac{3}{4}(x-1) + \tfrac{1}{4}(x-1)^3, \; 1 \le x \le 2$$

$$\underline{S}_1(x) = 3 + \tfrac{3}{2}(x-2) + \tfrac{3}{4}(x-2)^2 - \tfrac{1}{4}(x-2)^3, \; 2 \le x \le 3$$

Table 3 showcases the application of different linear algebra techniques to determine the loop currents in Experiment 3's electric circuit problem. Direct methods like Gaussian Elimination and Gauss-Jordan Elimination, alongside iterative approaches such as Jacobi and Gauss-Seidel, were employed. These methods yield crucial insights into electric circuit analysis, elucidating how electric charge flows through the circuit's branches. Interpretations of the obtained loop currents, denoted as $I_1 = 2.06A$, $I_2 = -0.41A$, and $I_3 = 0.22A$, provide clarity on current distribution, voltage drops, and power dissipation within the circuit. Such insights facilitate advancements in electrical engineering, aiding in circuit analysis, design, and troubleshooting by discerning component behavior and assessing circuit performance. Direct methods like Gaussian elimination and Gauss-Jordan elimination provide precise solutions efficiently, suitable for complex circuit configurations. These methods guarantee accurate results but have a computational complexity of O(n^3). In contrast, iterative methods such as Jacobi and Gauss-Seidel offer advantages for large-scale circuit problems, with a computational complexity of O(n^2). Although iterative methods may converge slowly, they are more suitable for systems with numerous equations.

Table 4 depicts the flow pattern or general solution that describes the flow of the traffic system in experiment 4. Examining the flow pattern, it is observed from a practical point of view that all flow must be non-negative and this force $x_4 \le 300$

The unknowns in experiment 4 stand in for different sections or segments of the downtown road network. The numbers assigned to these unknowns in Table 4 indicate the traffic flow (in vehicles per hour) along each road segment. Each unknown $(x_1, x_2, x_3, x_4 \; and \; x_5)$ corresponds to a particular road segment. For example, the variables x_4 indicates freely fluctuating variables, and $x_1, x_2, x_3 \; and \; x_5$ reflect flow values on specific streets, respectively. The traffic patterns and directional flow

along these route segments are depicted in Table 4. Comprehending the road network's flow pattern is essential to enhancing traffic control tactics, enhancing transportation effectiveness, and mitigating urban congestion. Therefore, in order to improve the efficiency and security of urban transport systems, policymakers and urban planners can make better decisions by examining the flow patterns of road networks. Experiment 4 provides insights into the flow pattern of vehicles in a traffic network, offering practical implications for traffic system management. By analyzing the flow pattern, transportation authorities can identify congestion points, optimize signal timings, and improve overall traffic efficiency. This information informs decision-making in traffic management, leading to reduced travel times and enhanced transportation functionality. Therefore, the findings from Experiment 4 contribute to the development of strategies for mitigating congestion and improving urban transportation networks.

Recognizing the inherent constraints and assumptions within each application field is crucial when practically integrating linear algebra into areas such as traffic flow analysis, cubic spline interpolation, genetics, and electric circuits. The accuracy of genetic predictions depends on factors such as the complexity of genetic models, data availability, and assumptions regarding genetic inheritance patterns. In cubic spline interpolation, the assumptions of continuity and smoothness may be challenged by noisy or sparse data. In electric circuit analysis, simplifying circuit models is common, leading to discrepancies between theoretical predictions and real-world behavior. Similarly, traffic flow analysis often simplifies real-world traffic systems, assuming uniform traffic conditions and homogeneous behavior. Acknowledging these constraints enhances study transparency, aids in interpreting findings, and directs future research towards resolving these issues, thereby increasing the adaptability of linear algebraic approaches across various contexts.

4 CONCLUSION

In conclusion, this study delved into the practical integration of linear algebra across various domains, including genetics, cubic spline interpolation, electric circuits, and traffic flow analysis. Through detailed methodologies and analyses, key insights were gained. The investigation of genetic distributions over generations provided understanding of evolutionary processes and inheritance patterns. The

application of cubic spline interpolation facilitated precise data representation and curve fitting in diverse fields. Electric circuit analysis showcased the importance of linear algebra techniques in understanding current flow, voltage distribution, and circuit performance. Additionally, traffic flow analysis highlighted the role of linear systems in modeling and optimizing transportation networks. Overall, this study underscores the profound impact of linear algebra in solving complex real-world problems and advancing understanding across multiple disciplines, paving the way for future research and innovation in interdisciplinary studies. The implications of this research emphasize the indispensability of linear algebra in addressing complex real-world problems across diverse domains. By harnessing the computational power and analytical rigor of linear algebra, researchers and practitioners can gain deeper insights into the underlying mechanisms of biological systems, develop more accurate predictive models, design efficient electrical systems, and optimize transportation infrastructures. Ultimately, the integration of linear algebra contributes to advancements in science, engineering, and technology, driving innovation and progress in the modern world.

Conflict of Interest

There is no conflict of interest between the authors.

Authors Contributions

In the context of this research paper, Khadeejah James Audu formulated the conceptual framework and played a key role in shaping the methodology. Yak Chiben Elisha was instrumental in preparing the data and drafting the content, while Yusuph Amuda Yahaya provided valuable supervision throughout the project. Sikirulai Abolaji Akande contributed by thoroughly reviewing and editing the manuscript.

Acknowledgment and Support

Statement of Research and Publication Ethics

The study is complied with research and publication ethics.

REFERENCES

[1] H. A. Abdulmohsin, H. B. Abdul Wahab, and A. M. Jaber Abdul Hossen, "A Novel Classification Method with Cubic Spline Interpolation", *Intelligent Automation & Soft Computing*, vol. 31, no. 1, pp. 780-863, 2022.

[2] K. M. M. Aburaas, "Matrices and their Applications in Electrical Circuits", *African Journal of Advanced Pure and Applied Sciences (AJAPAS)*, pp. 364- 370, 2023.

[3] S. Andrilli and D. Hecker, *Elementary linear algebra*. Academic Press, Elsevier, Netherlands, 2022.

[4] M. Ashraf, V. De Filippis, and M. A. Siddeeque, *Advanced Linear Algebra with Applications*. Springer Nature Singapore, Gateway East, Singapore, 2022.

[5] M. L. De Klerk and A. K. Saha, "A review of the methods used to model traffic flow in a substation communication network", *IEEE Access*, vol. 8, pp. 204545-204562, 2020.

[6] W. Hao, D. Rui, L. Song, Y. Ruixiang, Z. Jinhai, and C. Juan, "Data processing method of noise logging based on cubic spline interpolation", *Applied Mathematics and Nonlinear Sciences*, vol. 6, no. 1, pp. 93–102, 2021.

[7] A. D. Madhuri, P. V. N. Sagar, P. G. Raju, and A. A. Tanuja, "A Study on Applications of Linear Algebra", *Mathematical Statistician and Engineering Applications*, vol. 71, no. 4, pp. 2463-2473, 2022.

[8] C. D. Meyer and I. Stewart, "Matrix analysis and Applied linear algebra", Society for Industrial and Applied Mathematics (SIAM), 2023.

[9] M. M. Moghaddama, "11th Seminar on Linear Algebra and its Applications", arXiv preprint arXiv:2206.05494, 2022.

[10] T. T. Moh, "Linear Algebra and its Applications", *Monatshefte für Mathematik*, vol. 199, pp. 929-931, 2022.

USING SWARA METHOD FOR EVALUATION OF FACTORS AFFECTING PEDESTRIAN SAFETY AT INTERSECTIONS

Nuriye Kabakuş [1] (iD), **Merve Eyüboğlu** [2],* (iD)

[1] *Atatürk University, Faculty of Applied Sciences, Department of Emergency Aid and Disaster Management, Erzurum, Türkiye, nsirin@atauni.edu.tr*
[2] *Atatürk University, Graduate School of Natural and Applied Sciences, Department of Civil Engineering, Erzurum, Türkiye, merve.eyuboglu95@gmail.com*
* *Corresponding author*

KEYWORDS

ARTICLE INFO

ABSTRACT

Intersections are considered among the most hazardous points in traffic and can pose significant dangers, especially for pedestrians. The primary aim of this study is to investigate factors affecting pedestrian safety at intersections and to develop effective strategies to enhance pedestrian safety. In this context, various factors influencing pedestrian safety at intersections need to be considered. Within the scope of the research, factors such as pedestrian speed, vehicle speed, traffic signs and signals, intersection geometry, signaling systems, road surface, traffic volume, illegal parking, weather and lighting conditions, pedestrians' ages and clothing choices have been identified as key elements affecting pedestrian safety at intersections. These criteria have a wide range of impacts on traffic safety. The SWARA method was used to determine the priority order of these criteria. As a result of this analysis, vehicle speed was identified as the most significant factor, while pedestrian clothing choice was determined to be the least important factor. Based on the analysis of these criteria, appropriate measures can be taken to ensure safe pedestrian crossings. In conclusion, a holistic approach must be adopted to enhance pedestrian safety. This entails considering all factors affecting pedestrian safety at intersections and developing appropriate strategies. This approach can lead to more effective solutions to intersection safety issues and ensure pedestrian safety.

1   INTRODUCTION

Road transportation has brought many problems in parallel with the increasing population. Considering the economic and environmental losses due to the increase in traffic density in metropolitan and metropolitan areas, it is observed that the focus of the problems is the intersections [1]. Intersections, which are the separation and joining points of highways, are the most important elements of the road network that ensure the safe transfer of traffic flow. They are critical points in terms of accident risk. When traffic accidents are analyzed, it is seen that intersections play a major role and it has been examined that they pose a hazard to the safety of pedestrians.

There are three basic factors in traffic accidents: human, vehicle and environment (road). Human beings are at the top of these elements. Pedestrians, known as the most vulnerable road users, have always been seriously affected by accidents [2]. More than 1/5 of the people who die on highways around the world die as pedestrians. In order to protect pedestrians and ensure safe travel, understanding the risk factors in pedestrian crashes and successful interventions are required. In this context the parameters that can affect pedestrian safety at critical intersections have been determined as a result of the necessary investigations. The higher the speed at which the vehicle is traveling, the higher the risk of hitting the pedestrian and the vehicle. Likewise, the higher and uncontrolled the pedestrian's speed, the greater the risk of an accident as it will affect the vehicle's road and stopping distance relationship. Another important factor that affects the safe and orderly flow of traffic by directing pedestrians and drivers correctly in traffic is traffic signs and traffic sign boards [3]. The fact that the traffic sign boards are adequate and in accordance with the standards and their meanings are known by road users will positively affect pedestrian safety at intersections [4]. Intersections can be configured in different ways according to their geometric characteristics. Roundabouts are preferred more than level intersections in terms of traffic and pedestrian safety.

Signalization applications are one of the important factors that positively affect pedestrian safety by ensuring the regular flow of traffic at intersections, which are key points of traffic [5]. The road is the foundation of traffic. For this reason,

the geometric characteristics of the road are important for the safety of traffic and pedestrians. The pavement type of the road is affected by climatic conditions and traffic load depending on whether it is flexible or rigid. Deformations such as wheel tracks, holes, settlements and undulations on the road pavement will increase the risk of accidents [6]. Heavy traffic volume will negatively affect pedestrian travel. This reduces the safety of the pedestrian. Misparking negatively affects the traffic in motion and the pedestrian's travel passage.

When the weather is good and road conditions are favorable, the risk of fatal accidents is higher otherwise, the risk of fatal accidents is lower. In addition, more vehicles are on the road when the weather is clear and fewer vehicles are on the road when the weather is bad. On slippery surfaces with bad weather, the grip force of the tires will decrease, vehicles will start to slip and the risk of accidents will increase. Therefore, the density of traffic volume is considered negative for the safety of pedestrians at intersections [7]. The fact that daytime travel is higher than nighttime endangers safety due to the volume of traffic. The speed of pedestrians is affected by their gender and age. As age increases, crossing speeds decrease [8-16]. Young adults and younger pedestrians tend to violate the rules more than pedestrians in other age groups [17-18]. As drivers, young people are also more prone to errors than older individuals. Pedestrians' choice of light-colored clothing has a negative impact on safety as it increases the time it takes for daytime drivers to notice and react. Pedestrians' choosing dark-colored clothes more is among the precautions to be taken against a possible accident.

This study presents an MCDM approach to examine the factors affecting pedestrian safety at intersections and to develop strategies to improve pedestrian safety. SWARA method is used as an MCDM approach. Based on the literature, 12 criteria affecting pedestrian safety at intersections are evaluated by SWARA method. In the evaluation process, expert opinions form the basis for the analysis method. According to Zavadskas et al. the advantages of the SWARA method are primarily seen in the fact that there are far fewer comparisons compared to other criteria and that experts' opinions on the importance of the criteria are evaluated in the process of determining the weights of the criteria. Thanks to these features, this method is applied in many different fields.

Following this introduction, the article is divided into five sections. The next section presents a brief summary of the literature on pedestrian safety at intersections, while Section 3 provides a brief description of the material and the methodology used in the study. Section 4 summarizes the analysis results of the SWARA method and Section 5 summarizes the main conclusions of this study.

Edigbe et al. [19] aimed to determine the level of service of signalized intersections on the highway. In the study, average delay was used as intersection performance parameter. As a result of the analysis, it was found that the absence of signals at roundabouts effectively reduces intersection congestion and conflicts and improves the level of service. Wang et al. [20] and Muffert et al. [21] stated in their studies that geometric features can be of great benefit when analyzing traffic safety and driver behavior at roundabouts.

In their study, Öksüz and Eyigün [22] addressed the problems of Bahçelievler Ünverdi Intersection in Istanbul and proposed projects related to the existing geometry of the intersection. In his study, Montella [23] states that at least one geometric factor is effective in 60% of the total accidents at roundabouts. This finding suggests that the design of geometric elements at roundabouts plays a critical role in traffic safety. The aim of this review study is to analyze the relationship between roundabout geometric elements and safety performance in the light of the research conducted to date. It also evaluated the situation in Turkey and the motivation for this study was motivated by the lack of previous detailed studies on the subject.

Murat and Çakıcı [4] investigated whether the drivers in Denizli have sufficient knowledge and awareness about traffic signs and signals. The 27 traffic signs and signals that are frequently encountered in daily life were selected and a questionnaire consisting of 27 questions was created for 500 people who drive vehicles. According to the evaluations, it was observed that 40% had medium, low and very low level of awareness and 25% of the traffic signs had very high level of awareness. This situation was evaluated negatively in terms of traffic signs and markings. If the public is not sufficiently aware of traffic signs and markings, accidents will be inevitable. In this context, public awareness should be raised through education and mass media.

Quddus et al. [24] combine the sequential response model with econometric analysis to investigate the relationship between road traffic safety and crash severity. In this study, other contributing factors were controlled for when examining crash records and a traffic density measure was used with non-clustered crash data. This study highlights the importance of using sequential response models and econometric analysis in the field of road traffic safety.

2 MATERIAL AND METHOD

2.1 Material

Pedestrians are the most vulnerable group in traffic accidents and intersections are particularly risky areas for pedestrians. In this context, this study examines various factors affecting pedestrian safety at intersections. The criteria used in the study include twelve different criteria: pedestrian speed (C1), vehicle speed (C2), traffic sign boards (C3), intersection geometry (C4), signalization (C5), pavement type (C6), traffic volume (C7), misparking (C8), weather condition (C9), day status (C10), pedestrian age (C11), pedestrian's choice clothing (C12 (Figure1)).
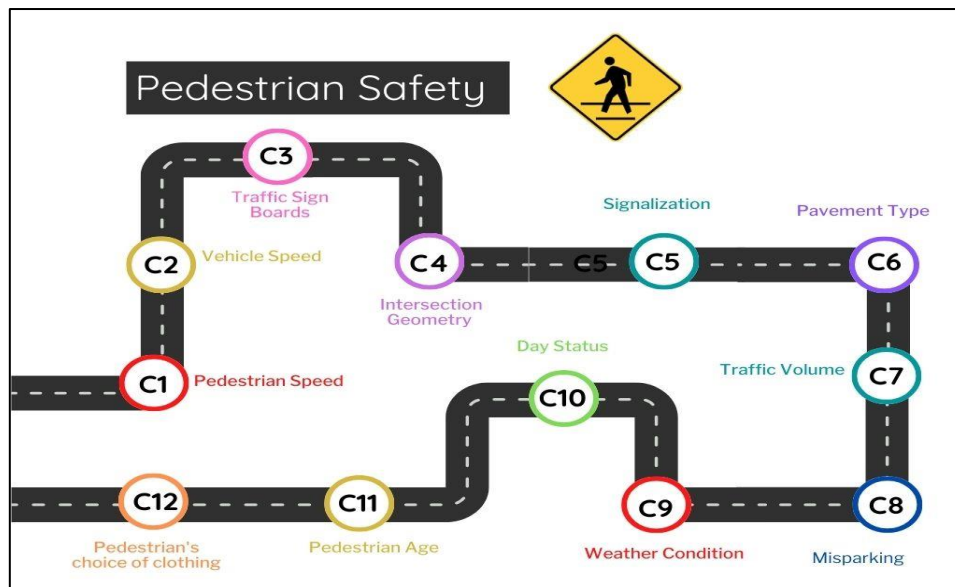

Figure 1. The criteria used in the study

2.2   Method

SWARA (Step-wise Weight Assessment Ratio Analysis) method, one of the Multi-Criteria Decision Making (MCDM) method, was used in the study. For the analysis, literature reviews and expert opinions (a group consisting of 4 academicians and 1 master engineer in transportation engineering) were used. In the interviews with the experts, they were asked to rank the importance of the criteria used in the study in terms of pedestrian safety at intersections and according to this ranking, their opinions were obtained about how much more important each criterion is than the previous criterion. In this study, SWARA method was used in Microsoft Excel. SWARA method was applied for weighting the criteria. A brief description of the method used is given below.

2.3   SWARA (Step-wise Weight Assessment Ratio Analysis) Method

SWARA method is one of the methods for determining weight values that play an important role in the decision-making process [25]. SWARA is a multi-criteria decision-making (MCDM) method that is simple and highly suitable for working with experts. SWARA is an effective tool in complex decision-making processes and performs a step-by-step analysis to determine the weights of various criteria and alternatives. In this method, the opinions of experts play an important role in the calculation of criteria weights [26-27]. Figure 2 shows the flowchart of this study.
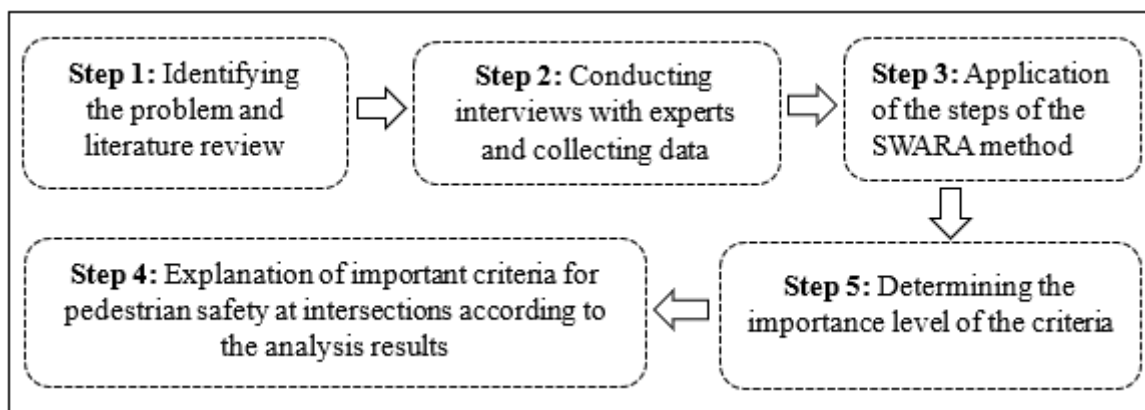
Figure 2. *The flowchart of this study*

The process of determining criterion weights is presented in Figure 3.
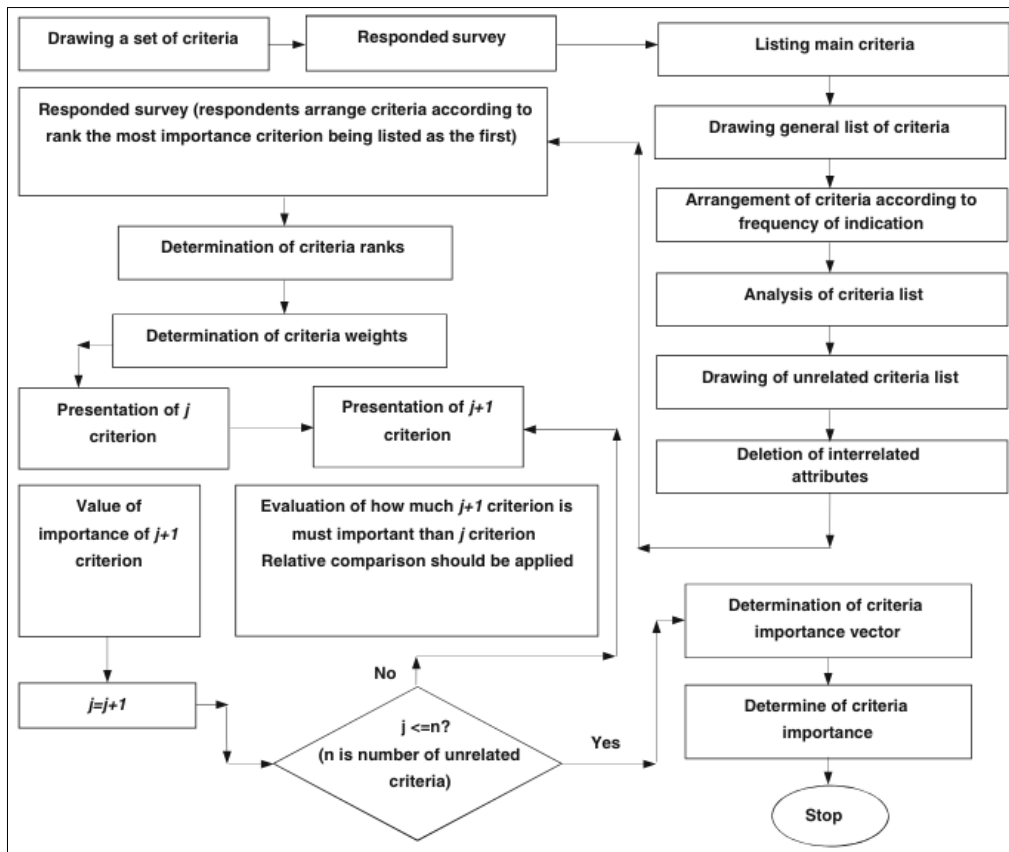
Figure 3. The proposed flowchart of the SWARA method [26]

The steps of the relative weighting process of criteria using the SWARA method are listed below [28].

Step 1: The criteria are simply listed in descending order of importance in line with expert opinion. If more than one expert will evaluate the criteria, the criteria are ranked in descending order as a result of the evaluation made by each expert, and a general ranking is created by taking the geometric mean of the criteria [29].

Step 2: The relative importance of each criterion is determined. For this (j+1). with criterion j. By comparing criteria; j. criterion (j+1). The importance of the criterion is expressed as a percentage. This value was determined by Kersuliene et al. [26] denoted by sj and called 'comparative importance of the average value'.

Step 3: The kj coefficient is determined as in equation 1.

$$k_j = \begin{cases} 1 & j = 1 \\ sj + 1 & j>1 \end{cases}$$

(1)

Step 4: qj variable is calculated with the equation in equation 2.

$$q_j = \begin{cases} 1 & j = 1 \\ \dfrac{qj - 1}{kj} & j > 1 \end{cases} \tag{2}$$

Step 5: The relative weights of the evaluation criteria are determined by equation 3. Here wj, j. indicates the relative weight of the criterion.

$$w_j = \frac{qj}{\sum_{k=1}^{n} qk} \tag{3}$$

3   RESULTS AND DISCUSSION

The weighting of the criteria affecting pedestrian safety at intersections was determined using SWARA by establishing a decision-maker team of 5 from experts in the fields and the authors, as well as examining the literature. In the interviews with the decision makers (DM), they were first asked to rank the importance of the criteria affecting pedestrian safety at intersections. Then, they were asked to compare how much more important the criteria are in percentage terms than the next criterion in the ranking they determined. As a result of the interview, the importance rankings of the criteria and the comparative importance of the average value (sj) variable were obtained from the DM and the data set was created (Table 1). For the criteria in the data set (C1, C2, C3, C4, C5, C6, C7, C8, C9, C10, C11 and C12), kj and qj variables were calculated for each DM using Equation 1 and Equation 2 in the steps of SWARA method. Then, the relative weights of the criteria were calculated using Equation 3 (Table 1).

For example, decision maker-1 ranked the criteria as C2-C4-C7-C5-C8-C3-C1-C11-C9-C10-C6-C12 in descending order of importance starting from the most important criterion. According to DM-1, the most important criterion for pedestrian safety is C2, while the least important criterion is C12. Then, in order to determine the comparative importance of the average value (sj), DM-1 compared each criterion with the preceding criterion, such as the 2nd ranked criterion with the 1st ranked criterion, the 3rd ranked criterion with the 2nd ranked criterion, starting with the

2nd ranked criterion. DM-1 stated that C4 is 30% more important than C2 (Table 1). Table 1 shows the importance rankings and sj values of the criteria collected from the other DM in the same way. In order to determine the criteria weights (wj), kj and qj values are calculated using the equations given in the steps of SWARA method and given in Table 1.

Table 1. Criteria ranking obtained from decision makers and SWARA method variables

	Criteria	C2	C4	C7	C5	C8	C3	C1	C11	C9	C10	C6	C12
DM1	Order of	1	2	3	4	5	6	7	8	9	10	11	12
	sj		0,3	0,2	0,1	0,15	0,2	0,1	0,05	0,25	0,1	0,1	0,2
	kj	1	1,3	1,2	1,1	1,15	1,2	1,1	1,05	1,25	1,1	1,1	1,2
	qj	1	0,76	0,64	0,58	0,50	0,42	0,38	0,36	0,29	0,26	0,24	0,20
	wj	0,17	0,13	0,11	0,10	0,08	0,07	0,06	0,06	0,05	0,04	0,04	0,03
	Criteria	C2	C4	C7	C5	C3	C6	C8	C1	C11	C9	C10	C12
DM2	Order of	1	2	3	4	5	6	7	8	9	10	11	12
	sj		0,20	0,15	0,10	0,10	0,30	0,10	0,25	0,20	0,20	0,10	0,20
	kj	1,00	1,20	1,15	1,10	1,10	1,30	1,10	1,25	1,20	1,20	1,10	1,20
	qj	1,00	0,83	0,72	0,65	0,59	0,46	0,41	0,33	0,27	0,23	0,21	0,17
	wj	0,16	0,14	0,12	0,11	0,10	0,07	0,07	0,05	0,04	0,03	0,03	0,03
	Criteria	C2	C4	C3	C5	C1	C11	C8	C7	C6	C9	C10	C12
DM3	Order of	1	2	3	4	5	6	7	8	9	10	11	12
	sj		0,15	0,2	0,1	0,1	0,05	0,1	0,1	0,2	0,1	0,3	0,2
	kj	1	1,15	1,2	1,1	1,1	1,05	1,1	1,1	1,2	1,1	1,3	1,2
	qj	1	0,87	0,72	0,65	0,59	0,57	0,51	0,47	0,39	0,35	0,27	0,22
	wj	0,15	0,13	0,10	0,09	0,09	0,08	0,07	0,07	0,05	0,05	0,04	0,03
	Criteria	C2	C7	C5	C4	C3	C8	C6	C1	C11	C9	C10	C12
DM4	Order of	1	2	3	4	5	6	7	8	9	10	11	12
	sj		0,3	0,2	0,15	0,1	0,1	0,1	0,1	0,2	0,1	0,2	0,25
	kj	1	1,3	1,2	1,15	1,1	1,1	1,1	1,1	1,2	1,1	1,2	1,25
	qj	1	0,76	0,64	0,55	0,50	0,46	0,41	0,38	0,31	0,28	0,24	0,19
	wj	0,17	0,13	0,11	0,09	0,08	0,08	0,07	0,06	0,05	0,05	0,04	0,03
	Criteria	C2	C5	C4	C9	C6	C3	C7	C1	C11	C12	C10	C8
DM5	Order of	1	2	3	4	5	6	7	8	9	10	11	12
	sj		0,3	0,25	0,05	0,7	0,15	0,1	0,45	0,7	0,15	0,4	0,75
	kj	1	1,3	1,25	1,05	1,7	1,15	1,1	1,45	1,7	1,15	1,4	1,75
	qj	1	0,76	0,61	0,58	0,34	0,3	0,27	0,18	0,11	0,09	0,06	0,03
	wj	0,22	0,17	0,14	0,13	0,07	0,06	0,06	0,04	0,02	0,02	0,01	0,00

Table 2 shows the weights calculated for each criterion for each DM using equation 3. For example, according to DM-2, the weight of criterion C2 is the highest, while the weight of criterion C12 is the lowest. According to DM-5, the weight of criterion C2 is the highest while the weight of criterion C8 is the lowest. Using the

weights obtained according to the DM, the importance ranking was made for each criterion by taking the geometric mean of these weights (Table 2).

Table 2. Importance ranking of criteria

Criteria	Decision Maker-1	Decision Maker-2	Decision Maker-3	Decision Maker-4	Decision Maker-5	Final Criteria Weights	Ranking
C1	0,068	0,057	0,090	0,066	0,043	0,063	7
C2	0,176	0,169	0,150	0,173	0,228	0,177	1
C3	0,074	0,101	0,109	0,088	0,068	0,087	5
C4	0,136	0,141	0,130	0,097	0,140	0,128	2
C5	0,103	0,111	0,099	0,111	0,175	0,117	3
C6	0,043	0,078	0,059	0,073	0,079	0,065	6
C7	0,113	0,122	0,071	0,133	0,062	0,096	4
C8	0,089	0,071	0,078	0,080	0,009	0,051	10
C9	0,052	0,039	0,054	0,050	0,133	0,059	8
C10	0,047	0,036	0,041	0,042	0,016	0,034	11
C11	0,064	0,047	0,086	0,055	0,025	0,051	9
C12	0,036	0,030	0,034	0,033	0,022	0,031	12

Table 2 shows the weights of the criteria affecting the affecting pedestrian safety at intersections. As a result of the weighting, the most important criterion was C2-vehicle speed. The least important criterion was the C12-pedestrian's choice of clothing. The order of importance was C2-C4-C5-C7-C3-C6-C1-C9-C11-C8-C10-C12.

This study seems to examine a set of criteria using the SWARA method to evaluate pedestrian safety at intersections. According to the literature review, similar comprehensive studies that assess pedestrian safety by integrating such a multitude of criteria are rarely encountered. This may underscore a significant advantage of the selected criteria and the SWARA method. The results suggest that both the selected criteria and the country-specific conditions could contribute positively to the literature. This study could be a valuable resource for researchers aiming to develop more effective strategies to enhance pedestrian safety at intersections.

4   CONCLUSION AND SUGGESTIONS

Traffic accidents, one of the problems brought about by the developing and changing world, cause millions of people to lose their lives every year. Most of these accidents occur at intersections and this situation poses a serious risk, especially for pedestrians, who are the most vulnerable group in accidents. Intersections are the most intense points of interaction between vehicles and pedestrians. Pedestrian safety has a key role in preventing traffic accidents. It is of great importance to ensure pedestrian safety at intersections for the safety of both pedestrians and other road users. Therefore, identifying and prioritizing criteria to improve pedestrian safety at intersections is an important step.

In the study, the criteria affecting the safety of pedestrians at intersections were determined as a result of literature reviews and ranked by SWARA method by taking the opinions of experts. The study includes twelve different criteria such as pedestrian speed, vehicle speed, traffic sign boards, intersection geometry, signalization, pavement type, traffic volume, misparking, weather condition, day status, pedestrian's age, pedestrian's choice of clothing. According to the results of the analysis obtained by applying the SWARA method, the order of these criteria starting from the most important one is; vehicle speed, intersection geometry, signalization, traffic volume, traffic signs and markings, pavement type, pedestrian speed, weather, pedestrian's age, pedestrian's age, misparking, day condition and pedestrian's choice of clothing. The selection of these criteria highlights the main objective of the study, which is to improve pedestrian safety at intersections. These choices aim to play a pioneering role in the field and represent an exemplary approach to intersection safety. Strategies and measures that can be implemented to improve pedestrian safety at intersections:

- Individuals can be educated from an early age to increase knowledge and awareness about traffic.

- Reviewing the geometry of intersections, the location of pedestrian crossings and signage is important to improve pedestrian safety. In particular, pedestrian crossings should be clear and distinct, pedestrian crossings should be widened, safe pedestrian zones should be created at intersections and pedestrians should be given priority.

- Awareness can be raised by providing information about traffic in mass media.

- Speed-breaking measures should be taken when approaching intersections to keep vehicle speeds under control. Signalization systems should be installed and actively used at specific and needed intersections.

- Traffic signs and markings should be actively used to keep traffic in a regular and safe flow.

- With the use of sensors at intersections and the integration of smart traffic systems, new technological solutions can be developed for pedestrian safety. For example, warning systems can be installed for the presence of pedestrians at the intersection.

As a result, sustainable solutions should be proposed to increase pedestrian safety at intersections and cooperation should be established with the necessary stakeholders to implement the solutions. Thus, important steps will be taken to reduce traffic accidents and ensure pedestrian safety.

Conflict of Interest Statement

There is no conflict of interest between the authors.

Authors Contributions

Nuriye Kabakuş: Investigation, Methodology, Writing - original draft, Writing - review & editing, Visualization.

Merve Eyüboğlu: Conceptualization, Methodology, Software, Validation, Formal analysis, Investigation, Writing - original draft, Writing - review & editing.

Statement of Research and Publication Ethics

The study is complied with research and publication ethics.

REFERENCES

[1] Y. Özinal and V. E. Uz, "Evaluation of the effect of roundabout geometric elements on intersection safety in the light of the literature," *Polytechnic Journal*, Vol. 24, no. 1, pp. 283-297, 2021, https://doi.org/10.2339/politeknik.630947

[2] A. Ünal and M. Saplıoğlu, "Micro-level investigation of the effects for pedestrian-pedestrian and pedestrian-vehicle interactions and other factors on crossing speed in pedestrian crossings," *International Journal of Engineering Research and Development*, Vol. 13, no. 1, pp. 113-126, 2020, https://doi.org/10.29137/umagd.736604

[3] S. Janpla, P. Bumrugrad, K. Kularbphettong, "Developing a traffic-sign knowledge application on android system," *Procedia-Social and Behavioral Sciences*, Vol. 191, no. 2015, pp. 680-685, 2015, https://doi.org/10.1016/j.sbspro.2015.04.559

[4] Y. Ş. Murat and Z. Çakıcı, "A research on the awareness of traffic signs: Denizli example," *BEU Journal of Science*, Vol. 6, no. 1, pp. 21-30, 2007.

[5] B. D. Brabender and L. Vereeck, "Safety effects of roundabouts in flanders: Signal type, speed limits and vulnerable road users," *Accident Analysis and Prevention*, Vol. 39, no. 3, pp. 591-599, 2007, https://doi.org/10.1016/j.aap.2006.10.004

[6] M. A. Kurt, "Traffıc sign signals measuring awareness," M. S. thesis, Dept. Civil Eng., Tokat Gaziosmanpaşa Universitiy, Turkey, Tokat, 2020.

[7] A. Bek, "Investigation of fatal and injury traffic accidents occurring on the Istanbul-Ankara state highway in 2004, depending on weather conditions, road surface conditions and direction conditions on the road," M. S. thesis, Dept. Civil Eng., Gazi University, Turkey, Ankara, 2007.

[8] W. Daamen and S. P. Hoogendoorn, "Pedestrian free speed behavior in crossing flows," *In Traffic and Granular Flow*, Springer, pp. 299-304, 2007, https://doi.org/10.1007/978-3-540-47641-2_25

[9] N. Garbera and L. Hoel, "Traffic and highways engineering," *West Publishing Company*, Virginia, USA, 2009.

[10] M. A. Granie, M. Pannetier, L. Gueho, "Developing a self-reporting method to measure pedestrian behaviors at all ages," *Accident Analysis and Prevention*, Vol. 50, pp. 830-839, 2013, https://doi.org/10.1016/j.aap.2012.07.009

[11] G. Ren, Z. Zhou, W. Wang, Y. Zhang, W. Wang, "Crossing behaviors of pedestrians at signalized intersections," *Transportation Research Record:Journal*

of the Transportation Research Board, Vol. 2264, 65-73, 2011, https://doi.org/10.3141/2264-08

[12] L. Asher, M. Aresu, E. Falaschetti, J. Mindell, "Most older pedestrians are unable to cross the road in time: a crosssectional study," Age Ageing, Vol. 41, no. 5, pp. 690-694, 2012, https://doi.org/10.1093/ageing/afs076

[13] S. Chandraa, A. S. Bhartib, "Speed distribution curves for pedestrians during walking and crossing," *Procedia-Social and Behavioral Sciences*, Vol. 104, no. 2, pp. 660 -667, 2013, https://doi.org/10.1016/j.sbspro.2013.11.160

[14] P. Önelçin, "Examining pedestrians' crossing behavior at signalized intersections and determining their safe distance perceptions," M. S. thesis, Dept. Civil Eng., Ege University, Turkey, İzmir, 2014.

[15] S. Dündar, "Analysis of pedestrian crossing speed-the case of İstanbul," *ICE Publishing*, Vol. 170, no. 1, pp. 29-37, 2017, https://doi.org/10.1680/jmuen.15.00036

[16] M. Saplıoğlu, A. R. Faisal, "Evaluation of pedestrian crossing behavior in signal-controlled and uncontrolled sections," *Gümüşhane University Journal of Science*, Vol. 10, no. 2, pp. 309-320, 2020.

[17] E. M. Díaz, "Theory of planned behavior and pedestrians' intentions to violate traffic regulations," *Transportation Research Part F*, Vol. 5, no. 3, pp. 169-175, 2002, https://doi.org/10.1016/S1369-8478(02)00015-3

[18] C. Holland and R. Hill, "The effect of age, gender and driver status on pedestrians intentions to cross the road in risky situations," *Accident Analysis and Prevention*, Vol. 39, no. 2, pp. 224-237, 2007, https://doi.org/10.1016/j.aap.2006.07.003

[19] B. J. Edigbe, A. Eltwati, I. Abbaszadehfallah, "Extent of delay and level of service at signalized roundabout," *International Journal of Engineering & Technology*, Vol. 2, no. 3, pp. 419-424, 2012.

[20] B. Wang, D. A. Hensher, T. Ton, "Safety in the road environment: a driver behavioural response perspective," *Transportation*, Vol. 29, no. 3, pp. 253-270, 2002, https://doi.org/10.1023/A:1015661008598

[21] M. Muffert, D. Pfeiffer, U. Franke, "A stereo-vision based object tracking approach at roundabouts," *IEEE Intelligent Transportation Systems Magazine*, Vol. 5, no. 2, pp. 22- 32, 2013, https://doi.org/10.1109/MITS.2013.2244934

[22] M. İ. Öksüz, Y. Eyigün, "Effects of geometric arrangements on pedestrian traffic and vehicle traffic (Bahçelievler example)," *Journal of Technology and Applied Sciences*, Vol. 5, no. 2, pp. 49-63, 2022, https://doi.org/10.56809/icujtas.1150104

[23] A. Montella, "Analysis of crash contributory factors at urban roundabouts," Transportation Research Board 89th Annual Meeting, Washington DC, 2010.

[24] M. Quddus, C. Wang, S. Ison, "Road traffic congestion and crash severity: Econometric analysis using ordered response models," *J. Transp. Eng.*, Vol. 136, no. 5, pp. 424-435, 2010, https://doi.org/10.1061/(ASCE)TE.1943-5436.0000044

[25] D. Radović, Ž. Stević, "Evaluation and selection of KPI in transport using SWARA method," Transport&Logistics: *The International Journal*, Vol. 8, no. 44, pp. 60-68, 2018.

[26] V. Kersuliene, E. K. Zavadskas, Z. Turskis, "Selection of rational dispute resolution method by applying new step-wise weight assessment ratio analysis (SWARA)," *Journal of Business Economics and Management*, Vol. 11, no. 2, pp. 243-258, 2010, https://doi.org/10.3846/jbem.2010.12

[27] M. R. G. Nezhad, S. H. Zolfani, F. Moztarzadeh, E. K. Zavadskas, M. Bahrami, "Planning the priority of high tech industries based on SWARA-WASPAS methodology.:The case of the nanotechnology industry in İran," *Ekonomska istrazivanja*, Vol. 28, no. 1, pp. 1111-1137, 2015, https://doi.org/10.1080/1331677X.2015.1102404

[28] D. Stanujkic, D. Karabasevic, E. K. Zavadkas, "A Framework for the selection of a packaging desing based on the SWARA method," *Inzinerine Ekonomika-Engineering Economics*, Vol. 26, no. 2, pp. 181-187, 2015, https://doi.org/10.5755/j01.ee.26.2.8820

[29] A. Ruzgys, R. Volvaciovas, C. Ignatavicius, Z. Turskis, "Integrated evaluation of external wall insulation in residential building using SWARA-TODIM MCDM method," *Journal of Civil Engineering and Management*, Vol. 20, no. 1, pp. 103-110, 2014, https://doi.org/10.3846/13923730.2013.843585